Inorganic chlorine budget and gas-particle partitioning in the winter lower troposphere over the northeast United States

Jessica D. Haskins

A thesis

submitted in partial fulfillment of the

requirements for the degree of

Master of Science

University of Washington

2017

Committee:

Joel Thornton

Lyatt Jaeglé

Becky Alexander

Program of Authorized to Offer Degree:

Atmospheric Sciences

University of Washington

Abstract

Inorganic chlorine budget and gas-particle partitioning in the winter lower troposphere over the northeast United States

Jessica D. Haskins

Chair of the Supervisory Committee:

Professor Joel Thornton

Atmospheric Science

Reactions of halogens occurring in fine mode aqueous aerosols are regulated by aerosol pH and liquid water content which affect ozone concentrations, tropospheric oxidant concentrations, sulfate and nitrate aerosol mass loadings, and hydrocarbon concentrations. However, the rates of heterogeneous and aqueous halogen reactions under atmospheric conditions, and, consequently the inorganic tropospheric halogen budget and its overall impact on air quality, remain highly uncertain. In this work, measurements from the 2015 Wintertime Investigation of Transportation, Emissions, & Reactivity (WINTER) aircraft campaign are used to show that the inorganic chlorine budget is dominated by HCl (g) and total particulate chloride, accounting for greater than 85% of the total chlorine budget within the boundary layer. The total amount and the range of all chlorine compounds sampled are elevated in marine environments with the total mass of inorganic chlorine compounds found over marine regions being 1014 pptv and 609 pptv over continental regions. The median observed mass fraction of chlorine in the fine mode

particle phase (pCl^-) is 0.054 ($Q_{25\%}$ = 0.038, $Q_{75\%}$ = 0.084) for the whole campaign, with large variability about this average. $ClNO_2$ was observed to peak at night containing ~15% of the overall chlorine budget (>1000 pptv). HOCl was observed to peak during the day and with a median of 100.8 pptv over the ocean and 21.3 pptv over land.

WINTER observations of gas and particle composition were used as inputs to the offline thermodynamic equilibrium model, ISORROPIA II, to compare observed and modeled chlorine gas-to-particle partitioning. Observations show 0-20% of available, submicron non-refractory chlorine partitions into the particle (0 - 0.2 $\mu g\ m^{-3}_{amb}$) at sufficiently high relative humidities, low temperatures, and pH above 0.8. The thermodynamic model significantly over-predicted particulate chloride by approximately a factor of two and under-predicted gas phase HCl by the same. Errors in the modeled HCl gas-particle partitioning may be caused by the presence of unmeasured refractory sodium chloride. The chlorine partitioning can be brought into agreement with the observations without significantly perturbing the nitrate partitioning by artificially increasing fine mode sodium chloride particle mass in the model to simulate an unmeasured sea salt fraction by $<0.1 \mu g\ m^{-3}$ in the median. The disagreement could also be caused by an over prediction in the effective equilibrium constant for HCl. An implied equilibrium constant function is derived from the WINTER data set and ISORROPIA II estimates of pH, LWC, and activity (K_{eq}= 4.5533 x 10^6 exp[3012 (1/T- 1/T_0)] $mol^2\ kg^{-2}_{soln}\ atm^{-1}$) which has a distinctly lower temperature dependency than the ISORROPIA II default value and is expected to be a lower limit of the equilibrium constant. Ultimately this work highlights the sensitivity of chlorine partitioning predictions by ISORROPIA II to minor changes chemical and environmental inputs. Such sensitivity will ultimately propagate to predictions of heterogeneous halogen chemistry and its effects on air quality and climate.

1 INTRODUCTION

In the last 20 years, halogens have been discovered to exert a significant influence on the chemical composition of the troposphere, affect the fate of pollutants in the atmosphere, and meaningfully impact climate [Simpson, et al 2015]. Specifically, multiphase chlorine chemistry has been shown to affect methane, ozone, and particle concentrations, all of which are influential climate forcing agents [Long et al,. 2010; Katzman et al., 2010; Thornton et al., 2010; Sarwar et al., 2014]. These effects result from the high reactivity of atomic chlorine radicals and chlorine oxides towards inorganic and organic compounds in the atmosphere [Riedel et al., 2014; Sherwen et al., 2016], and their coupling to the odd hydrogen (HO_x= OH+HO_2) and nitrogen oxide (NO_x=NO+NO_2) radical, which both regulate ozone concentrations and predominantly control the overall oxidative capacity of the atmosphere. Unlike other dominant oxidant pathways in the atmosphere, heterogeneous reactions between gas-phase species and halides on surfaces are centrally important to chlorine chemistry.

It is their low tropospheric concentrations, the key role of heterogeneous reactions, and the highly reactive nature of chlorine compounds and their precursors, which complicates the ability to measure them and, therefore, quantify their influence on the atmosphere and climate. Direct observations of elevated inorganic chlorine gases in coastal air were only first published in 1993 via mist chamber measurements [Pszenny et al., 1993] and to date, published observations of tropospheric inorganic chlorine gases are extremely limited. Global models have attempted to incorporate recent advances in our understanding of the impact of inorganic chlorine chemistry and their ultimate impact on air quality and climate in the troposphere [Long et al., 2010; Li et al., 2016; Sherwen et al., 2016]. However, they all point out that the heterogeneous chemistry of sea-salt and basic thermodynamic parameters needed to fully model the system are still highly

uncertain, that further field observations are needed as constraints, and that new modeling techniques need to be developed which are able to exploit those observational constraints [Saiz-Lopez et al., 2012b; Abbatt et al., 2012; Sander et al., 2015; Simpson et al., 2015; Sherwin et al., 2016].

This work presents results from the most expansive data set of inorganic chlorine compounds taken to date from the 2015 Wintertime Investigation of Transport, Emissions, and Reactivity (WINTER) aircraft campaign, and uses this data set to verify the ability of an existing thermodynamic model, ISORROPIA II, to explicitly predict equilibrium partitioning of chlorine between the gas and particle phases. Extensive comparisons of inorganic chlorine measurements are made to the limited record of prior measurements and found to be in generally good agreement. I show that the model's ability to accurately represent heterogeneous chlorine chemistry is extremely sensitive to often ignored or poorly constrained trace species like submicron sodium chloride. Although total sodium chloride mass concentrations can be measured with current techniques, its size distribution and submicron fraction are often not, and often measurement of sodium chloride remain low time resolution challenging analyses made aboard aircraft. While the submicron fraction of NaCl is expected to be small, I further show that even low concentrations can impact pH enough to affect ISORROPIA II's prediction of submicron chloride gas-particle partitioning while not affecting nitrate or ammonium concentrations. Ultimately, I show that while there is good potential for the coupling of ISORROPIA II to a global model to fully assess the global impact of halogen chemistry on air quality and climate. I conclude with a recommendation for future measurements in this regard to focus on comprehensive and simultaneous, high time resolution measurements of gases and size resolved aerosol composition that include trace species like submicron sodium chloride.

2 BACKGROUND

2.1 Sources of inorganic chlorine in the atmosphere & phase partitioning

The primary source of reactive chlorine in marine air and globally is from the emission of inorganic particulate chloride (pCl^-) from sea-salt aerosol spray produced at the ocean's surface via bursting bubbles. However, the concentration of pCl^- varies over several orders of magnitudes as a strong function of wind velocity and sea surface temperature [Graedel and Keene, 1995, Jaeglé et al., 2011], and concentrations decrease sharply above the marine boundary layer. Continental sources of reactive chlorine include aerosol production from salt plains or swimming pools and the direct emission of hydrochloric acid (HCl (g)) from power plants, but these sources are *much* smaller than their counterparts over the ocean [Keene et al., 1999]. The inland transport of super-micron sea salt aerosols is nearly negligible since they have a relatively short lifetime against deposition (~1.5 days) [Erikson et al., 1999; Keene et al., 1999]. However, submicron sea salt has a lifetime of 1-2 weeks and can be transported inland further making it a potentially important source even in areas not immediately adjacent to an ocean [Tegan et al, 1997].

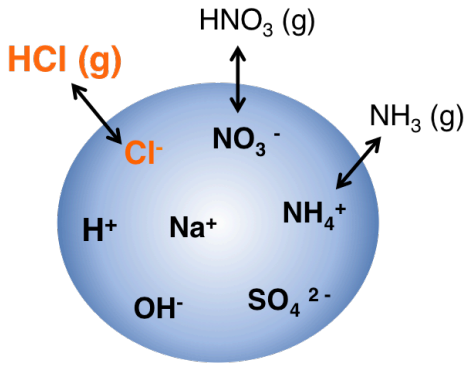

Figure 1: Illustration of the possible phase partitioning of chlorine, nitrate, and ammonia between their dissociated form in a deliquesced aerosol particle and in their forms in the gas phase

In addition to the inorganic sources of reactive chlorine, there are also tropospheric sources of reactive chlorine from organic precursors called chlorocarbons, such as dichloromethane (CH_2Cl_2) and chloroform ($CHCl_3$). Extremely reactive atomic chlorine radicals can be released from the oxidation and

photolysis of such organic chlorine species, which increase the amount of total reactive chlorine available in the troposphere through the coupling of photolytic halogen cycles and multiphase chemistry described in more detail in the following section and in **Figure 2**. A recent modeling study has estimated chlorocarbon oxidation pathways account for 0- 50% of tropospheric atomic chlorine radicals (~ 0-10 pptv). They estimate the smallest contributions from the oxidation of organic chlorine species to the radical chlorine atom budget within the wintertime marine boundary layer (<10%, ~0-1 pptv) [Hossaini et al., 2016]. Within the framework of this study, considering the halogen budget within the polluted marine boundary layer during the winter, the impact of these organic chlorine sources is expected to be small.

At Equilibrium:

$HCl\,(g) \longleftrightarrow HCl\,(aq)$ (R1)

$HCl\,(aq) \longleftrightarrow H^+\,(aq) + Cl^-\,(aq)$ (R2)

$$K_{EQ} = \frac{[H^+][Cl^-]\,\gamma_{H+}\gamma_{Cl-}}{P_{HCl}}$$

At typical atmospheric conditions, HCl(g) can exist in equilibrium with its hydrated form in the aerosol (**R1**) . However, as a strong acid, it undergoes rapid dissociation yielding H^+(aq) and Cl^- (aq) (**R2**). This equilibrium can be perturbed by the partitioning of other acids such as HNO_3 and H_2SO_4 into the aerosol. As other acids are taken up into the particle, they can quickly displace chloride from the aerosol in the form of HCl(g) by affecting the acidity of the particle and thereby the dissociation equilibrium of HCl and by affecting the anionic composition on the activity coefficients [Chameides and Stelson, 1992]. The volatilization of HCl from primarily marine aerosol via acid displacement reactions is estimated to be the largest global source of HCl [Keene et al., 1999].

The equilibrium partitioning of chlorine between the gas and particle is also reversible, and in areas where nitrate and sulfate are less abundant, HCl can be taken up into the particle, where it rapidly dissociates, yielding particulate chloride (pCl^-) available for subsequent reaction in the liquid (**R1-R2**). Indeed, a recent study has hypothesized that inland, where the sources of

particulate chloride are small, partitioning of HCl emitted from anthropogenic sources like power plants into the particle could provide a source of pCl^- significant enough to propagate subsequent reactions at levels previously thought only to be relevant over the ocean [Reidel et al., 2013].

The phase partitioning of chlorine, nitrate, and ammonium is regulated by aerosol size, particle pH, liquid water content, water and solute activity (γ), and ambient temperature and pressure. **Figure 1** shows the possible equilibrium partitioning between the gas and particle for multiple compounds. Deliquesced fine mode aerosols are often highly concentrated, and thus non-ideal, salt solutions. Therefore, the equilibrium partitioning of all species is greatly impacted by the activity coefficients of the various ions in solution. Within the polluted marine boundary layer, the pH of submicron aerosols is primarily determined by the bulk sulfate, nitrate, and ammonium contributions because they are present in much larger concentrations in the aerosol than chloride, sodium or alkaline earth metals as shown by Guo et al., 2015, Guo et al., 2016, and Guo et al., 2017. The typical pH of submicron aerosols sampled within this environment has been shown to be extremely acidic, with values ranging from -1 to 3 [Keene et al., 1998; Geo et al., 2015; Guo et al., 2016; Guo et al., 2017]. It is the small volumes of the fine mode aerosol that allows such low pH values to be achieved.

In less polluted areas, the chemistry that governs chlorine activation from sea spray aerosol is less well understood. Laskin et al. 2012 suggests that acid displacement processes involving low-volatility organic acids may play an important role in HCl volatilization from the particle in such areas. In the absence of large amounts of nitrate or sulfate, it is also possible that trace species from mineral dust could contribute to fine particle pH, which would tend to raise the pH of the particles, but the observational dataset needed to verify this is somewhat limited. Guo et al 2017 compared all fine particle pH estimates made to date in different seasons across

the US and in the Mediterranean with varying ranges of bulk nitrate and bulk sulfate and showed that all studies have consistently found highly acidic submicron particles with pH generally less than 3.

The typically low pH of fine mode aerosol is important because both the partitioning of nitrate and chlorine, which are coupled through their mutual dependence on aerosol pH, between the gas and the particle span a range from 0-100% at atmospherically relevant temperatures, pressures, and relative humidities between pH=-1 to 3. Thus, in order to explicitly predict available fine mode particulate chloride or HCl concentrations (as well as particulate nitrate or HNO_3) in the lower troposphere, the equilibrium of a Cl^--Na^+-SO_4^{2-}-NH_4^+- NO_3^- - water inorganic aerosol system must be solved. Existing global models that include halogen chemistry do not solve this thermodynamic equilibrium to predict available particle chloride or gas phase HCl. Sherwen et al., 2016, which implemented gas phase tropospheric halogen chemistry in GEOS-Chem, specifically notes that not including the acid displacement of HCl in the model is one primary source of uncertainty in halogen budget of the lower boundary layer.

2.2 Significance of subsequent multiphase chloride reactions

There are numerous ways to convert particulate chloride into reactive chlorine gas phase compounds, which impact air quality, climate, and the overall tropospheric oxidant budget, which are briefly summarized in **Figure 2**. Ultimately, it is critical to correctly model pCl^- because various multiphase halogen reactions that liberate chlorine from the particle are central to the photochemical cycling of other reactive chlorine compounds in the gas phase. For example, one way to liberate particulate chloride that couples to the cycling of nitrogen oxides in the atmosphere is tied to the formation of nitryl chloride ($ClNO_2$). It is a photolabile reservoir of

Cl atoms and NO_x that forms via the heterogeneous reaction of dinitrogen pentoxide (N_2O_5) on chloride containing aerosols (R2), and is understood to be especially important in the winter.

$ClNO_2$ production & photolysis

$N_2O_5\ (g) + Cl^-\ (aq) \rightarrow (2\text{-}\phi)\ HNO_3\ (g) + \phi\ ClNO_2\ (g)$ (R3)

$ClNO_2\ (g) + h\nu \rightarrow Cl^{\bullet} + NO_2\ (g)$ (R4)

$ClNO_2$ builds up in the boundary layer at night when N_2O_5 levels are high and undergoes photolysis in the morning (**R3**) to produce atomic chlorine radicals ($Cl^{\bullet}$) and NO_2, both of which have significant impacts on the atmosphere [Platt et al., 2004, Mielke et al., 2013, Cooper et al., 2010, Thornton et al., in prep] $ClNO_2$ is relatively unreactive at night when it is formed, and acts as a reservoir species, transporting NO_x downwind of its sources in polluted areas. Upon sunrise, the photolysis of $ClNO_2$ acts as a net NO_x source in rural or remote regions (**R4**).

This redistribution of NO_x by $ClNO_2$ is particularly important in the winter and can ultimately impact whether a region is net producing or destroying ozone. In winter, the production of hydroxyl radicals (OH), the most important atmospheric oxidant, is considerably slower owing to changes in photolysis rates. This ultimately leads to a slowdown in the concurrent oxidation of primary pollutants like NO_x and VOCs, which leads to a slow down in the well-known phenomenon of photochemical ozone production in near-source regions (**R5-R8**).

Photochemical ozone production

$OH + RH \rightarrow RO_2 + H_2O$ (R5)

$RO_2 + NO \rightarrow R'O + HO_2 + NO_2$ (R6)

$HO_2 + NO \rightarrow OH + NO_2$ (R7)

$2x\ (NO_2 + h\nu \rightarrow NO + O_3)$ (R8)

N_2O_5 formation & loss

$2x\ (NO + O_3 \rightarrow NO_2 + O_2)$ (R9)

$NO_2 + O_3 \rightarrow NO_3 + O_2$ (R10)

$NO_2 + NO_3 \rightarrow N_2O_5$ (R11)

$N_2O_5 + H_2O\ (l) \rightarrow 2HNO_3$ (R12)

The slow down in photochemical ozone production in near source regions during winter, in combination with the nighttime formation and loss N_2O_5, a process that depletes ozone, can lead to the net destruction of ozone in near-source regions where NO_x is readily available to

participate in this chemistry (**R9-R12**). Owing to the aforementioned decrease in the availability of OH during winter, because NO_x oxidizes far more slowly, broader background levels of NO_x accumulate and consequently spread over wider geographic areas downwind of sources. In these downwind regions, despite the reduction in available OH, it has been suggested that the increase in background NO_x levels in winter can result in net production of ozone [Yienger et al., 1999]. The production of $ClNO_2$ and subsequent release of NO_x would serve to increase the production of ozone in downwind areas. Estimates of the magnitude of this effect range from global decreases of the tropospheric O_3 burden by 18.6% in GEOS-Chem v10-01 [Sherwin et al., 2016], a decrease of 65% in the boundary layer O_3 concentrations in CAM v3.6.33 [Long et al., 2013], and an increase of the boundary layer O_3 concentrations by 16.3% in WRF-Chem [Li et al., 2016], but calls for more dynamic means of parameterizing $ClNO_2$ production are found across the literature. Ultimately, $ClNO_2$ production and transport during winter is key to understanding the interplay between near source ozone destruction and widespread ozone production and a robust, accurate means of solving the equilibrium phase partitioning of chlorine is critical to accurately represent it.

Beyond its impact on NO_x and ozone, the early morning release of atomic chlorine radicals when $ClNO_2$ photolyzes has other important atmospheric implications, especially in winter. Because chlorine radicals are highly reactive with VOCs, they decrease their lifetimes and potentially enhance the secondary organic aerosol (SOA) loading of the atmosphere. Sherwin et al., 2016 points out that the oxidation of VOCs like ethane, acetone and propane by chlorine atoms can be globally significant accounting for ~15-27% of their loss. Reidel et al., 2013 and other work underway from the WINTER 2015 campaign indicate that chlorine atoms

can be *the* primary oxidant in the early morning in winter when OH production can be both lower in magnitude and more slowly produced.

In addition to the oxidation of VOCs, the chlorine radicals released from the photolysis of $ClNO_2$ can also react with O_3 to form the radical, hypochlorite ($ClO^{\bullet}$). From there, $ClO^{\bullet}$ can undergo a self-reaction to form molecular chlorine (Cl_2), which rapidly photolyzes, yielding two chlorine radicals while catalytically destroying ozone, as it does in the stratosphere. Or, $ClO^{\bullet}$ can undergo reactions with NO_2 or HO_2 to form different, non-radical reservoirs, either chlorine nitrate ($ClNO_3$ (g)) or hypochlorous acid (HOCl (g)), respectively. The photochemical cycling of these liberated chlorine compounds can then couple back to multiphase chemistry via the reaction of HOCl with particulate chloride, pCl^- in the condensed phase to produce Cl_2. The net effect of this cycle, which starts with one chlorine radical (and one HO_2 radical), is to produce two chlorine radicals. An analogous series of reactions involving bromine is termed the "bromine-explosion" since it is ultimately an autocatalytic cycle that builds up the pool of reactive halogen radicals in the atmosphere. But essentially, this series is just a conversion of HO_x radicals to Cl_x radicals through the combination of heterogeneous reactions involving pCl^- and photodissociation of Cl_2 that ultimately consumes protons from the aqueous phase shifting the pH of aerosol surfaces to be less acidic [Simpson et al., 2015]. On a final note of the possible pathways that particle chloride can be "liberated" from the particle into the reactive gas phase, laboratory studies have shown that at sufficiently low pHs (<2), N_2O_5 can directly oxidize particulate chloride to Cl_2, which may be responsible for the production of molecular chlorine on acidic aerosol particles [Roberts et al., 2008]. However, magnitude of this effect, the rate and other key uncertainties remain.

Figure 2 summarizes the key pathways through which chlorine compounds cycle and

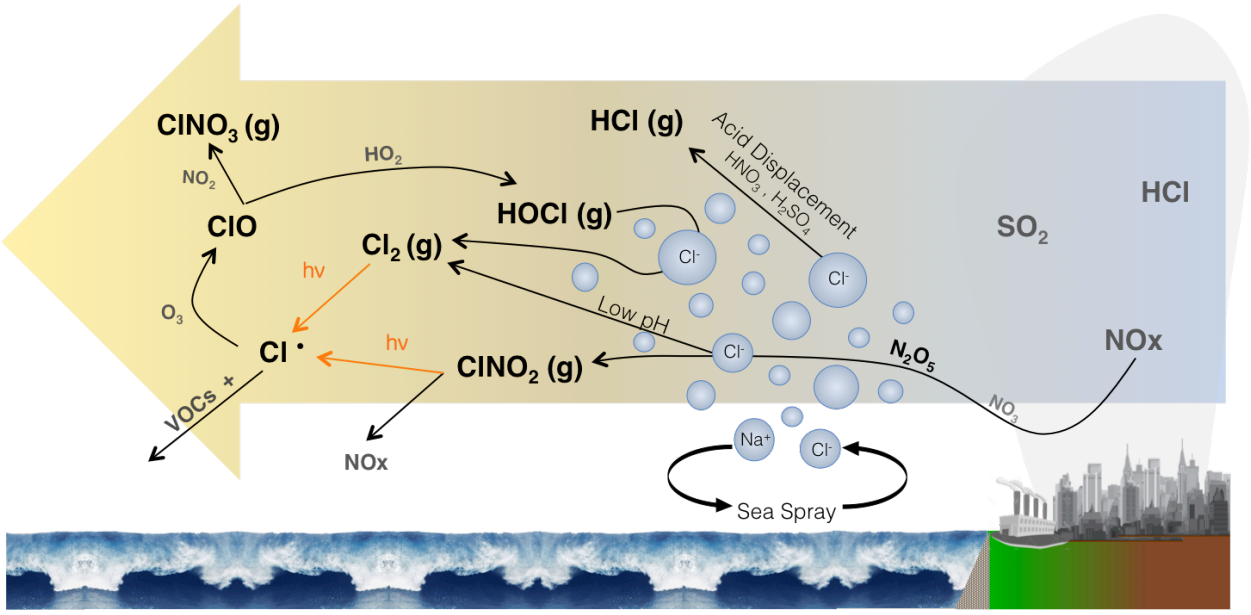

Figure 2: Figure summarizing the pivotal role of multiphase chlorine reactions in coupling the emission of local anthropogenic emissions to the downwind transport of NOx and morning release of oxidants via reactions involving the nighttime heterogeneous processing of N_2O_5, photolytic chlorine cycling, and acid displacement reactions.

highlights the pivotal role that particulate chloride plays in connecting the primary emission of pollutants to their downwind effects on the oxidant budget and distribution of NO_x. Ultimately, the production of all the inorganic reactive chlorine gases in the marine boundary layer arise through various chemical reactions that happen in sea-spray aerosols [Pszenny et al., 1993; Graedel and Keene, 1995; Sander and Crutzen, 1996; Vogt et al., 1996; Keene et al., 1998; Oum et al., 1998; Spicer et al., 1998; Erikson et al, 1999; Keene et al 1999]. The accurate representation of nearly all the relevant chlorine species in the gas phase that affect tropospheric ozone concentrations and the tropospheric oxidant budget in global models require an accurate and thorough representation of particulate chloride because of the key role heterogeneous chemistry plays in halogen chemistry.

3. METHODS

3.1 Campaign & Instrumentation

One of three main focuses of the Wintertime Investigation of Transport, Emissions, and Reactivity, an NSF sponsored aircraft campaign that took place in February and March of 2015, was to understand how multiphase reactive nitrogen chemistry affects oxidant availability, ozone production, reactive halogen cycling, and the export of pollutants during winter. A rich suite of chemical compounds, including O_3, NO_x, $ClNO_2$, N_2O_5, HNO_3, NO_3, PAN, hydrocarbons, and aerosol composition were measured over 13 flights along the eastern US during the day and night above rural and highly populated areas. **Figure 3** shows the broad area sampled and the particular attention paid to capturing air masses downwind of coastal polluted regions throughout the night within the boundary layer when halogen heterogeneous processing occurs.

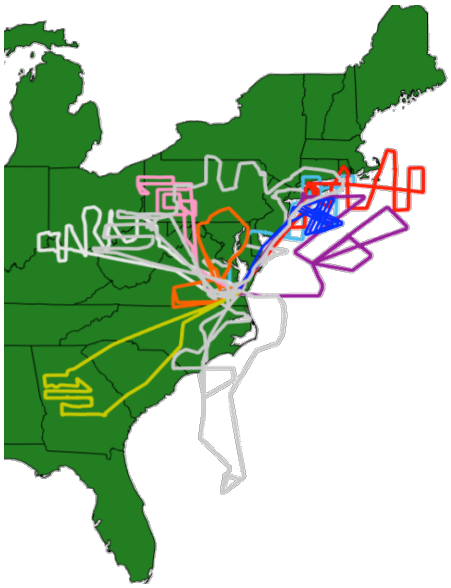

Figure 3: Flight path Map of WINTER 2015 campaign. Colors indicate flight paths that sampled air masses somewhat or entirely at night while grey flight paths were daytime only flights.

Onboard the NSF's C-130, outfitted with 28 different inlets, multiple instruments simultaneously sampled various gases, aerosol composition, photolysis frequencies, and particle size relevant to coupled nitrate and chlorine chemistry. In this work, focus will be given to data taken using the University of Washington's high resolution time of flight chemical ionization mass spectrometer (HR-ToF-CIMS), the University of Colorado's high resolution time of flight aerosol mass spectrometer (HR-ToF-AMS), and the University of New Hampshire's aerosol filter measurements, summarized in **Table 1**. The differences in these various aerosol composition sampling techniques, for reasons that will be shown, are particularly important to

correctly interpret the results of our modeling work, so added attention is paid to exactly w hat forms of particulate chloride are measured by each instrument.

Measurement	Instruments	Time Resolution	Reference
Various Gases (e.g. HCl, $ClNO_2$, HOCl, Cl_2, N_2O_5, HNO_3, etc.)	**University of Washington;** *Chemical Ionization Mass Spectrometry, I^-* **(CIMS)**	**2 Hz**	**Lee et al., 2014; Lopez-Hilifiker et al., 2016**
Submicron Aerosol Composition (non-refractory: pSO_4^{2-}, pNO_3^-, pCl^-, pNH_4^+)	**University of Colorado;** *Time of Flight Aerosol Mass Spectrometer* **(AMS)**	**1 Hz**	**Jayne et al., 2000; Jimenez et al., 2009;**
Supermicron Aerosol Composition (< 4 μm) (water soluble: pSO_4^{2-}, pNO_3^-, pCl^-, pNH_4^+, pNa^+)	**University of New Hampshire** *Filter Sampling*	**~ 5 min**	**Dibb et al., 1999; Dibb et al., 2000;**

Table 1: Table summarizing some of the measurements made during the WINTER 2015 aircraft campaign

3.1.1 CIMS

A high-resolution time-of-flight chemical ionization mass spectrometer (HR-ToF-CIMS) using iodide-adduct ionization, as described previously [B. H. Lee et al., 2014; Lopez-Hilfiker et al., 2016], was used to simultaneously detect HNO_3, HCl, $ClNO_2$, N_2O_5, Cl_2, HOCl, and $ClNO_3$ at 2 Hz. Iodide ions are produced by passing methyl iodide past a Po-210 foil and mixed with ambient air in a low pressure (80 mbar) flow reactor to selectively cluster with target gases in ambient air. A small fraction of the reaction mixture is continuously sampled into the mass spectrometer where they are separated by their time of flight detected. Calibrations for these various species are preformed through a variety of methods described in detail in Lee et al., 2014. For the WINTER campaign, calibrations of HCl were preformed through injection of a few microliters of an HCl/acetone solution with a known concentration onto a filter immediately upstream of the ion molecule reaction region. A flow of heated ultra-high purity N_2 is then passed over the filter to desorb the HCl. Integration of the signal and mass injected allow for a determination of the sensitivity. Calibrations to $ClNO_2$ were preformed in the field where N_2O_5 was quantified using the NOAA Atmospheric Ring-down Nitrogen Oxide Laser Detector (ARNOLD) instrument [Dubé et al., 2006; Fuchs et al., 2008] and then passed through a wetted

salt bed, generating $ClNO_2$. Assuming a 100% yield of $ClNO_2$ from **R3**, the amount of consumed N_2O_5, is used to calculate the sensitivity to $ClNO_2$. Previous measurements have shown that the UW-CIMS $ClNO_2$ and Cl_2 sensitivities (as determined using a permeation tube and cylinder) are very similar. HOCl was calibrated by quantitatively converting to Cl_2 by following the protocol of Foster et al 1999. Because a specific calibration to Cl_2 was not preformed during the WINTER campaign, we apply a similar sensitivity as we measured to $ClNO_2$. The relative measurement uncertainty for the reported data is estimated to be 50%, and detection limits vary flight to flight for each species. For the following analysis, values from the CIMS reported below zero are set to NaN and values below the determined detection limits are set to values equal to half of the detection limit.

3.1.2 Particle Composition Measurements

Non-refractory ions in particles with an aerodynamic diameter less than 1μm were sampled with a high-resolution time of flight aerosol mass spectrometer (HR-ToF-AMS) at 1 Hz in total aerosol mass mode. The general operation of the AMS has been described in detail previously [Jayne et al., 2000; DeCarlo et al., 2006; Canagaratna et al., 2007; Jimenez et al., 2009; Kimmel et al., 2011] and specifics about the operation of the HR-ToF-AMS during the WINTER campaign are described in Guo et al., 2016. Relative ionization efficiencies for sulfate, ammonium, nitrate, and chloride were determined by multiple in-field calibrations. Accuracy for AMS detection of inorganic species is estimated at 35% for aircraft operation [Bahreini et al., 2009]. Refractory species, such as salts like NaCl, $NaNO_3$, and Na_2SO_4, are inefficiently detected by the AMS [Hayes et al., 2013], meaning that the reported aerosol chloride measurement does *not* contain significant contributions from sea-salt. It was found that that HNO_3 (g) formed from nitrate evaporation reacted with residual chloride in the vaporizer resulting in a small extra

chloride signal needing corrections of -20% to the reported particulate chloride measurement and was adjusted accordingly in the results shown here.

In addition to the AMS particle composition measurement to account for missing refractory components of the aerosol like sea salt, water-soluble ions in particles with an aerodynamic diameter less than 1μm were sampled with a Particle-Into-Liquid-Sampler that was coupled with two Ion Chromatographs (ICs). Due to high baseline noise during the campaign, the cation IC was determined to have detection limits to high to confidently report measurements of NH_4^+ and Na^+ (comprehensive operational discussion provided in Guo et al., 2016). Therefore, only data from the anion IC was reported for the campaign (i.e. measurements of Cl^-, NO_3^-, SO_4^{2-}). Limits of detection (LOD) were estimated from blank measurements using a High Efficiency Particulate-Free Air filter taken during the first 10 minutes after take off of each flight. **Table 2** shows the estimated LODs, which were calculated as 3*x* standard deviation of the blanks for the PILS-IC for the two different time bases used in this work. The relative measurement uncertainty for the reported data is estimated to be 20%.

Unlike the PILS-IC, the AMS provides higher time resolution, a distinctly lower detection limit, and a more precise measurement of the suite of ions, since the same detector is used to sense both anions and cations. These issues are very relevant to this study. Guo et al., 2016 demonstrates that the AMS precision is most

	PILS 10s (5min)	AMS 10s (5min)	CIMS 10s (5min)
Nitrate (μg/m^3)	0.21 (0.04)	0.022 (0.004)	--
Sulfate (μg/m^3)	0.26 (0.05)	0.006 (0.001)	--
Chloride (μg/m^3)	0.51 (0.09)	0.022 (0.004)	--
Ammonium (μg/m^3)	--	0.003 (0.0006)	--
HCl (pptv)	--	--	22 (4.7)
HOCl (pptv)	--	--	1.0 (0.23)
Cl_2 (pptv)	--	--	0.1 (0.02)
$ClNO_2$ (pptv)	--	--	0.1 (0.03)

Table 2: List of the limits of detection of the PILS, AMS, and CIMS for various species for the two different sampling times 10 seconds and 5 minutes (shown in parenthesis) used in this work.

beneficial for assessing factors that influence pH where nitrate phase partitioning in concerned during the WINTER campaign, while the PILS accuracy is important for constraining the absolute value of pH, especially when nonvolatile cations are present.

Because the signal to noise ratio of the PILS cation IC was not sufficiently high to give meaningful measurements of sodium or ammonium, the AMS provided the only submicron measurement of ammonium, which is a critical buffering cation in a deliquesced aerosol in determining aerosol pH in the polluted marine boundary layer. Thus, in explicitly calculating the equilibrium partitioning of reactive chlorine a Cl^--Na^+-SO_4^{2-}-NH_4^+- NO_3^- - water inorganic aerosol system, a self-consistent, and relatively precise set of data was found to be more critical than the absolute concentrations of each aerosol constituent being correct (although the PILS-IC measurement was useful in constraining this) [Guo et al., 2016]. Similarly, I find that the precision of the AMS is extremely useful for assessing the factors that ultimately control chlorine phase partitioning, like aerosol pH. However, because HCl is a weaker acid than HNO_3, it is displaced from the aerosol first as pH changes making the equilibrium phase partitioning of reactive chlorine even more sensitive than the nitrate partitioning to issues raised by measurement uncertainty, accuracy, and precision. It was found that the particulate chloride concentrations rarely ever exceeded the detection limit of the PILS instrument, thus rendering its use in this study of gas to particle chlorine partitioning less useful than that of the HR-ToF-AMS. All submicron particulate chloride data used hereafter is that taken by the HR-ToF-AMS.

In addition to the two submicron aerosol sampling techniques deployed, a filter-sampling system was used to collect particles with an aerodynamic diameter estimated to be less than 5 μm, which were subsequently analyzed for water-soluble ions by IC, as previously described [Dibb et al., 1999; Dibb et al., 2000;]. One data point was collected from this method

approximately every 5 minutes. This aerosol composition measurement technique will capture supermicron contributions from sea-salt aerosols. Notably, this was the only technique that could sense any sodium contributions to aerosol mass during the WINTER campaign.

3.2 ISORROPIA II: Thermodynamic Equilibrium Partitioning Model

3.2.1 Model Description

In this work, the thermodynamic partitioning model, ISORROPIA II [Fountoukis and Nenes, 2007] was used to determine the composition and phase state of a Cl^--Na^+-SO_4^{2-}-NH_4^+-NO_3^- - water inorganic aerosol system in thermodynamic equilibrium using input data from the WINTER 2015 aircraft campaign. Using ISORROPIA II in an online global model like GEOS-Chem or WRF-Chem with total chloride input would specifically allow for a prediction of the acid displacement of HCl, particle pH, liquid water content, and particle chloride concentrations; all of which are important parameters for parameterizing the uncertainties in halogen heterogeneous chemistry. Previous work validating ISORROPIA II's ability to correctly predict gas-particle partitioning in the real atmosphere has not focused intently on its ability to do so for halogenated species, even if they are included in the inputs.

ISORROPIA II takes inputs of total (gas + particle) composition and ambient conditions and partitions species into either the gas or the particle in thermodynamic equilibrium with the system. For example, total chloride inputs to the model are the sum of the measured gas phase HCl from the UW-CIMS and a measurement of the particulate chloride from the AMS. Similarly, the total nitrate passed to the model would be the sum of HNO_3 and pNO_3^-. Inputs for species like sodium that do not partition into the gas phase, are taken as their observed particulate concentrations.

The model assumes thermodynamic equilibrium and distributes compounds into either the gas or the particle. Because particle and gas phase measurements were made separately during the WINTER campaign, it is then possible to verify whether the model has correctly partitioned those compounds. In addition to the normal outputs of particle and gas phase concentrations, we calculate particle pH following Guo et al., 2015 and Guo et al., 2016 as follows:

$$pH = -\log_{10} \gamma_{H+} H_{aq}^{+} = -\log_{10} \frac{1000\, \gamma_{H+} H_{air}^{+}}{W_i + W_o} \cong -\log_{10} \frac{1000\, \gamma_{H+} H_{air}^{+}}{W_i}$$

where γ_{H+} is the hydronium ion activity coefficient (assumed = 1, which could be evaluated using E-AIM), H_{aq}^{+} ($mole\ L^{-1}$) the hydronium ion concentration in particle liquid water, H_{air}^{+} ($\mu g\ m^{-3}$) the hydronium ion concentration per volume of air, and W_i and W_o ($\mu g\ m^{-3}$) are the particle water concentrations associated with inorganic and organic species, respectively. In this work, pH is calculated only considering the inorganic water contribution since the organic aerosol hygroscopicity was not measured during the WINTER campaign. Furthermore, Guo et al., 2016 shows that assuming an appropriate organic hygroscopic parameter for the WINTER campaign only increased pH by 0.07 units. Although this assumption does not significantly change the characterization of the overall pH of a submicron aerosol, I will show below that chlorine partitioning is particularly sensitive even to small changes in pH and this assumption's effects are further discussed in Section 5.

3.2.2 Model Simulations

ISORROPIA II inputs from WINTER campaign observations are described in **Table 3**. In addition, we use observations of ambient temperature, relative humidity and pressure. Two different runs were performed to investigate the trade offs in using different particle composition

data as part of the bulk input for reasons discussed in section 3.1.5. Only points where all inputs were measured with a finite value were run through ISORROPIA II. Furthermore, only submicron measurements of particle composition are passed to the model since the super-micron particles are much less likely to be internally mixed, a key assumption of the model. The best signal to noise ratio for the AMS data was found at a time resolution of 10s. Therefore, the equilibrium calculation is done for the 10s average of the input data for the entire WINTER campaign.

ISORROPIA Inputs	Guo et al. 2016 Base Case	This Work *Base + Cl*	This Work *Iterated NaCl*
Total Nitrate	CIMS HNO_3 + AMS NO_3^-	CIMS HNO_3 + AMS NO_3^-	CIMS HNO_3 + AMS NO_3^-
Total Sulfate	AMS SO_4^{2-}	AMS SO_4^{2-}	AMS SO_4^{2-}
Total Ammonium	AMS NH_4^+ + iterated NH_3	AMS NH_4^+ + iterated NH_3	AMS NH_4^+ + iterated NH_3
Total Chloride	0	CIMS HCl+ AMS Cl^-	CIMS HCl + iterated Cl^-
Sodium	0	0	iterated Na^+

Table 3: Table comparing inputs to ISORROPIA II from this study considering WINTER 2015 campaign chlorine partitioning and those from Guo et al., 2016 considering WINTER 2015 campaign nitrate partitioning and predicted fine particle pH

The first run was designed to closely mirror that done by Guo et al., 2016, but included total reactive chlorine (HCl + particulate Cl^-) as part of the inputs (simulation hereafter referred to as '*Base + Cl*'). Because there were no good-quality measurements of NH_3 (*g*) during the WINTER campaign, the bulk ammonia passed to the model (which should include NH_3(g) + NH_4^+ (aq)) was iterated in all simulations until the until the particle NH_4^+ prediction converged with observations. Guo et al., 2016 found that the amount of NH_3 needed was 0.1 ±0.34 $\mu g/m^3_{amb}$ and that most of the ammonia partitioned to the particle phase (~91% ± 22%) resulting in a systematic pH bias of ~0.2 pH units higher than runs that neglect this contribution. In my work, I find similar results when reactive chloride was added.

The second simulation preformed was identical to the *Base + Cl* run, except that aqueous sodium chloride concentrations were iterated until the predicted gas phase HCl came into agreement with the observations (simulation hereafter referred to '*Iterated NaCl'*). Total reactive chloride input was not allowed to be lower than CIMS HCl + AMS pCl^- (i.e. total reactive chlorine was added to account for missing fine mode sea-salt that the AMS could not detect, but the model was never allowed to run with less than that observed. At minimum, it ran with the original, observed AMS particulate chloride measurement). Any excess chloride added to account for the measurement model difference in gas-particle chlorine partitioning was assumed to be from sodium chloride, so equal molar amounts of sodium and chloride were added concurrently. In theory, adding sodium chloride would impact the amount of necessary total reactive ammonium needed by altering particle pH and since aqueous sodium chloride and NH_3 were simultaneously iterated, a correction to the amount of either NH_3 of particle chloride inputs would need to be made until both HCl and pNH_4^+ values simultaneously converged to their observations. Over 95% of all observations (n = 34022) passed to the model for evaluation resulted in values of NH_3, $Na^+(aq)$, $Cl^-(aq)$ for which mutual convergence of HCl and pNH_4^+ measurements with model predicted inputs was obtained. Convergence was required within 30 iterations for each observation with an average tolerance of either ± 10% of the measurement or ± 0.018 $\mu g/m^3_{amb}$ of NH_4^+ and ±15 pptv of HCl, which ever was largest. The same tolerance conditions were used in constraining only NH_3 in the *Base+Cl* simulation as well, with 98.5% of samples successfully converging on a solution. Only points that led to convergence on a solution that was able to match the measured values within tolerance are shown in comparisons presented below.

All ISORROPIA II runs performed assume that there is an aqueous phase present, gases and aerosols are in thermodynamic equilibrium, and particles are internally mixed across the size distribution, all of which have implications on our model output and the model-measurement chlorine partitioning agreement. I run ISORROPIA II in "metastable" mode, which suppresses any solid precipitates from forming. To ensure this is a realistic assumption for our inputs and following Guo et al., 2016, we exclude all data with RH < 20%; a condition where aerosols are less likely to be in a completely liquid state [Ansari & Pandis, 2000; Malm & Day, 2001; Fountoukis & Nenes, 2007]. Although conditions with RH panning the entire range from 0-118% were measured during the WINTER campaign, those with RH <20% and, therefore , excluded from analysis, represented about 20% of the data. It has also been shown that at such low relative humidities, the modeled activity coefficients associated with highly concentrated solutions are very uncertain [Fountoukis et al., 2009]. On the other end of the RH scale, owing to the exponential growth in particle liquid water with higher relative humidity, data with RH >95% are assumed to have a RH = 95%. Both uncertainties have been shown to affect the model predicted pH [Malm & Day, 2001, Guo et al., 2015, Guo et al., 2016] and therefore, partitioning of even major species like HNO_3 to the gas phase, but especially HCl (*g*), which, as a weaker acid, is even more sensitive to displacement from the particle as pH changes.

Several studies have shown that under ambient atmospheric conditions, submicron aerosols typically achieve equilibrium states within 30 minutes [Dassios and Pandis, 1999, Cruz et al., 2000, Fountoukis et al., 2009]. Although the WINTER campaign experienced conditions with low RH (<20%) and temperature (-21°C), when semi-solid and glassy states of inorganic semi-volatiles are theoretically possible, Guo et al., 2016 explicitly calculates the relevant equilibrium timescale and concludes that the aerosols observed remain in a deliquesced state

with rapid diffusion throughout the particle for the WINTER 2015 aircraft campaign, such that the inherent assumption of gas-aerosol equilibrium is valid.

4 RESULTS

4.1 Reactive Chlorine Budget

A summary of the total inorganic chlorine budget sampled during the WINTER 2015 campaign subdivided into air masses sampled over land and over the ocean below 1.5 km is shown in **Figure 4.** Only points where simultaneous measurement of all chlorine compounds (HCl(g), HOCl(g), Cl_2(g), $ClNO_2$(g), UNH pCl^-, PILS pCl^-) were made are included in this analysis. All statistics shown are calculated using data from a 5-minute average such that all of the measurements included in this analysis were representative of the same time base. Values where an individual measurement is found to be below the time averaging adjusted limit of detection are set to a value of ½ the detection limit (reported in **Table 2**) and are included in the analysis so that the median and average values reported are not biased high due to consistent samples of low concentrations below the detection limit. Negative values are assumed to be NaNs.

In both regions, the inorganic chlorine budget is dominated by HCl (g) and total particulate chloride (sampled by the filter, $D_p < 4\mu m$, shown in dark purple), accounting for greater than 85% of the total chlorine budget within the boundary layer. In line with expectations and published literature data, both the total amount and the range of all chlorine compounds sampled are elevated in marine environments [Graedel & Keene, 1995] with the total mass of inorganic chlorine compounds found over marine regions being 1014 pptv and 609 pptv over continental regions.

The amount of submicron water-soluble chloride ($D_p < 1\mu m$, sampled by the PILS-IC, shown in light purple) is shown to have the same median concentration over land and water with the range of values sampled is higher over land. However, both median concentrations of pCl^- are equal to ½ the detection limit of the PILS-IC since >50% of points sampled over land and water had very low pCl^- concentrations below the detection limits. The concentrations of *submicron* water-soluble chloride are not necessarily the same for continental and marine environments, but not different enough that it could be detected by the PILS-IC with its higher detection limit. The *total* amount of particulate chloride ($D_p < 4\mu m$, sampled by the filter, shown in dark purple) is distinctly elevated over the marine environments with median daily concentrations of 0.61 $\mu g \cdot m^{-3}_{amb}$ compared to 0.23 $\mu g \cdot m^{-3}_{amb}$ over land within the boundary layer. Therefore, the fraction of total chloride that is in the submicron is larger over land than over the ocean since the amount of total chloride is so much larger over the ocean.

HCl (g) measurements taken during the WINTER campaign represent one of the largest and broadest atmospheric sampling reported to date and are well in line with prior measurements and chlorine inventories both over the ocean and over land. The median mixing ratio of HCl observed during the WINTER campaign was 1014 pptv over the ocean and 435 pptv over land with a maximum of 3067 pptv over the ocean (averaged over 5 minutes). Sustained, elevated HCl concentrations were observed in the range of 1800 pptv in areas offshore on several flights (see **Figure 5**). The highest concentrations of HCl (> 5000 pptv) were measured during the WINTER campaign when directly sampling fresh coal-fired power plant plumes. Keene et al., 2007 reports HCl measurements taken off the coast of Maine in the summer of 2004 using a tandem mist chamber. They report maximum concentrations of 5728 ppt with a median value of 351 ppt and average of 599 ppt. This method of determination has a much slower time resolution

than sampling with the CIMS does and was a ground based campaign, so these composite statistics are reported from only 302 measurements that took place lower in the atmosphere than most of the WINTER measurements were taken. Although slightly lower values were reported on average in Keene et al., 2007, they are in generally good agreement given the scarcity of measurements of HCl in the boundary layer and distinctive differences in measurement technique.

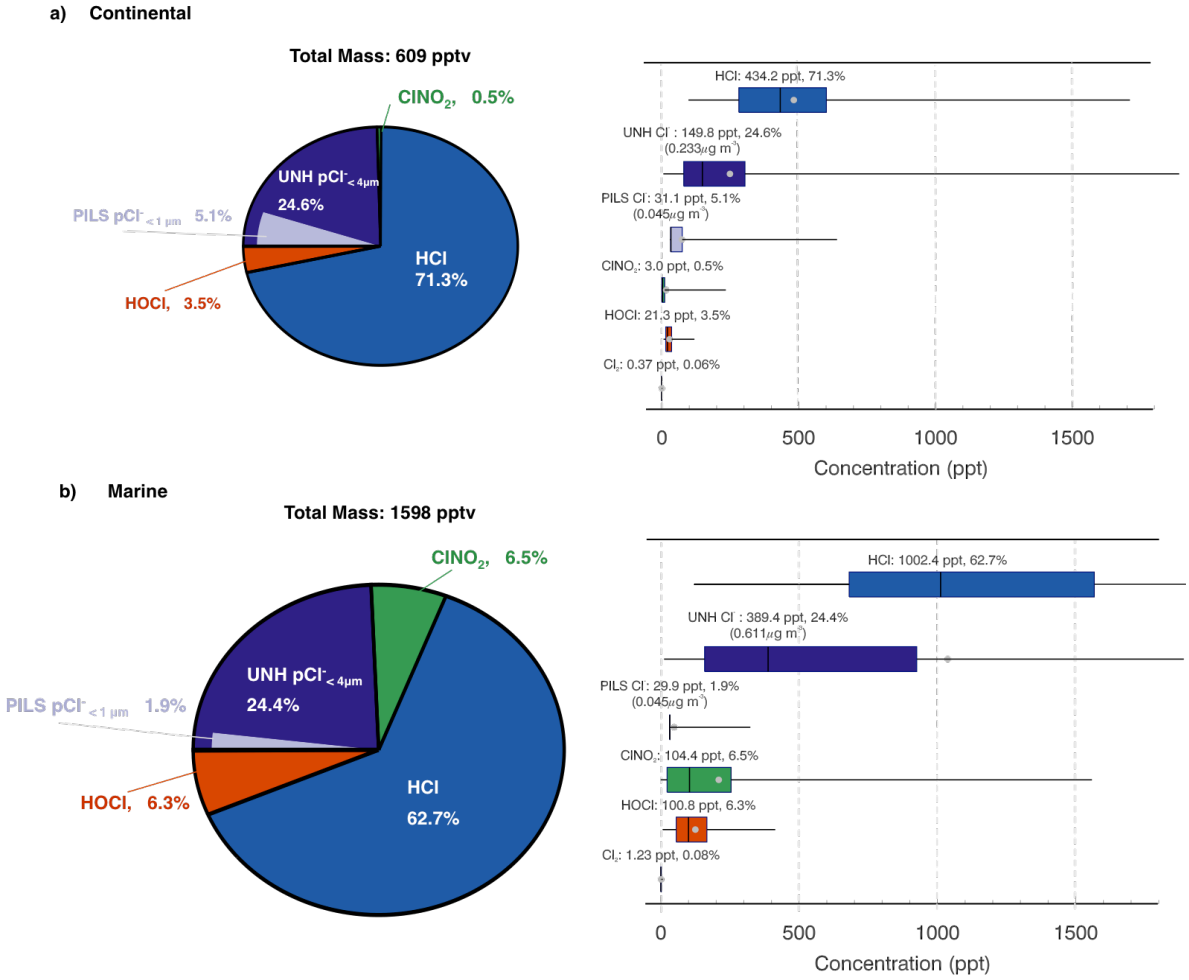

Figure 4: Median daily averaged values of the various inorganic chlorine compounds measured within the boundary layer (< 1.5 km) over land areas (panel a) and over the ocean (panel b). Averages shown as grey points in box and whisker plots. The table below summarizes the median and range of mixing ratios for various chlorine compounds < 1.5 km over continental and marine regions.

A suite of other inorganic chlorine compounds were measured during the WINTER campaign, generally at lower abundance compared to HCl, but having a higher reactivity in the condensed phase or due to photolysis. While $ClNO_2$ and HOCl both have distinctive diurnal cycles, it is notable that even averaged over an entire day they are still a significant fraction of the total chlorine budget in **Figure 4,** especially over the ocean. Subdividing the boundary layer chlorine budget into day and night, results look very similar to their daily averages over both the land and the ocean, but has $ClNO_2$ peaking at night as ~15% of the overall budget and HOCl peaking during the day similarly. Although, maximum $ClNO_2$ production is seen over the ocean as expected, it is important to note that concentrations of $ClNO_2$ seen within the boundary layer over land are not insignificant with plumes upwards of 70 ppt at night, which is enough to significantly impact the morning radical budget in the winter [Reidel et al., 2013].

An extensive review of the measurements of $ClNO_2$ in the marine boundary layer taken during the WINTER campaign is outside of the scope of this paper and is discussed in detail in several papers currently in preparation by other members of the WINTER campaign science

Continental / Marine	HCl	$pCl^-_{<4\ um}$(UNH)	$pCl^-_{<1\ um}$(PILS)	$ClNO_2$	HOCl	Cl_2
Min (pptv)	98.8	6.9	27.5	0.015	6.82	0.10
	121	13.3	28.2	0.05	7.08	0.10
$Q_{25\%}$ (pptv)	283	81.6	29.7	0.56	14.8	0.26
	683	160	29.2	23.4	56.3	0.68
Median (pptv)	435	150	31.0	2.96	21.3	0.37
	1014	389	30.0	104	101	1.23
$Q_{75\%}$ (pptv)	603	305	73.0	11.0	36.3	0.53
	1607	927	31.0	262	178	2.61
Max (pptv)	1712	1588	638	234	119	2.67
	3067	7436	325	1559	414	7.51

team. However, it is notable that measurements of $ClNO_2$ taken during the WINTER campaign are in generally good agreement in the overall pattern of the diurnal cycling and median boundary layer concentrations with all previous measurements of $ClNO_2$ data collected in both coastal and continental regions [Mielke et al., 2013, Tham et al., 2014, Riedel et al., 2012, Osthoff et al., 2008, Bannan et al., 2015, Faxon et al., 2015; Phillips et al., 2012, Thornton et al., 2010; Riedel et al., 2013, Mielke et al., 2011]. Recognizing that the WINTER campaign intentionally targeted areas where $ClNO_2$ production would be maximized, observations show large plumes forming offshore and downwind of polluted regions at night with maxims upwards of 1000 pptv.

A brief comparison of the HOCl and Cl_2 median day and night concentrations are made to prior literature here. Lawler et al., 2011 present measurements of HOCl and Cl_2 were made with an HR-ToF-CIMS using a bromine adduct ion at Cape Verde off the coast of Africa from May 30th-June 7th 2009, which was approximately 50 m from the ocean. They report distinctive diurnal trends with HOCl concentrations peaking during the day with an approximate daytime mean of 80ppt during only the first 4 days of the campaign with notably smaller diurnal trends and absolute concentrations during the half of the campaign.

The median WINTER HOCl concentration below 1.5 km over the ocean was 100.8 pptv, in good agreement with the first half of the Cape Verde measurements. Similarly, the continental median of HOCl concentrations during the WINTER campaign, which was 21.3 pptv below 1.5 km over the ocean, was slightly higher than the nighttime values reported in Lawler et al., 2011 during the first half of the campaign. However, both the marine and continental concentrations are consistently higher than nearly all the data points reported in the second half of the Cape Verde campaign. We initially estimate Cl_2 concentrations over an order of magnitude below

those reported throughout the Cape Verde campaign, but note that our Cl_2 measurement is a deliberately conservative estimate and only likely to increase. Previous modeling studies that attempt to compare to the Cape Verde campaign measurements found best agreement with second half of the campaign [Sherwin et al., 2016; Long et al., 2014], but note that their estimates of HOCl and Cl_2, which do not include explicit heterogeneous reactive chlorine chemistry, tend to underestimate those concentrations. The WINTER 2015 data set is the most comprehensive airborne observations of HOCl and Cl_2 taken in the atmosphere to date and could be very useful for testing model predictions of their spatial distribution. Because of the deliberately conservative estimates made for the calibrations, we can infer that the observed concentrations of these species in the atmosphere is likely larger than previously thought, but not completely outside of the absolute range of previous measurements.

Panel A in **Figure 5** illustrates the differences over the land and ocean in HCl concentrations. Over land, there are very distinctive point sources where power plant plumes in southern Pennsylvania and Georgia were sampled. They appear as large, isolated concentrations of anthropogenically emitted HCl that are slowly diluted downwind. However, over the ocean the background HCl levels are generally all elevated, suggesting widespread secondary chemical production of HCl, not primary emission. Panel B **Figure 5** shows the ratio of chloride to sodium by mass as measured by the UNH filter sized by the absolute amount of sodium available. In typical seawater, the ratio of chloride to sodium by mass is about 1.76- 1.80 [Junge et al., 1958]. If the ratio were depleted with respect to that of seawater, it is indicative of some chemistry removing chloride from the particle without removing sodium, as would occur via the acid displacement of HCl or equilibrium partitioning of HCl. This ratio is less useful if there is not any substantial amount of sodium available in the sampling region; thus, the each individual

point is sized by absolute sodium concentration. Aerosols (D_p<4 µm, UNH obs.) are significantly depleted in chloride with respect to the seawater ratio, specifically over the ocean, indicating some amount of secondary chemical processing removing chloride from the particle via volatilization. Similarly, the places with the highest levels of HCl over the ocean, correlate spatially very well with the areas where total particle chloride has been displaced from the particle relative to sodium. Panel C in **Figure 5** shows the chloride deficit of the UNH filter measurements, again sized by the absolute sodium concentration. It is defined as the difference

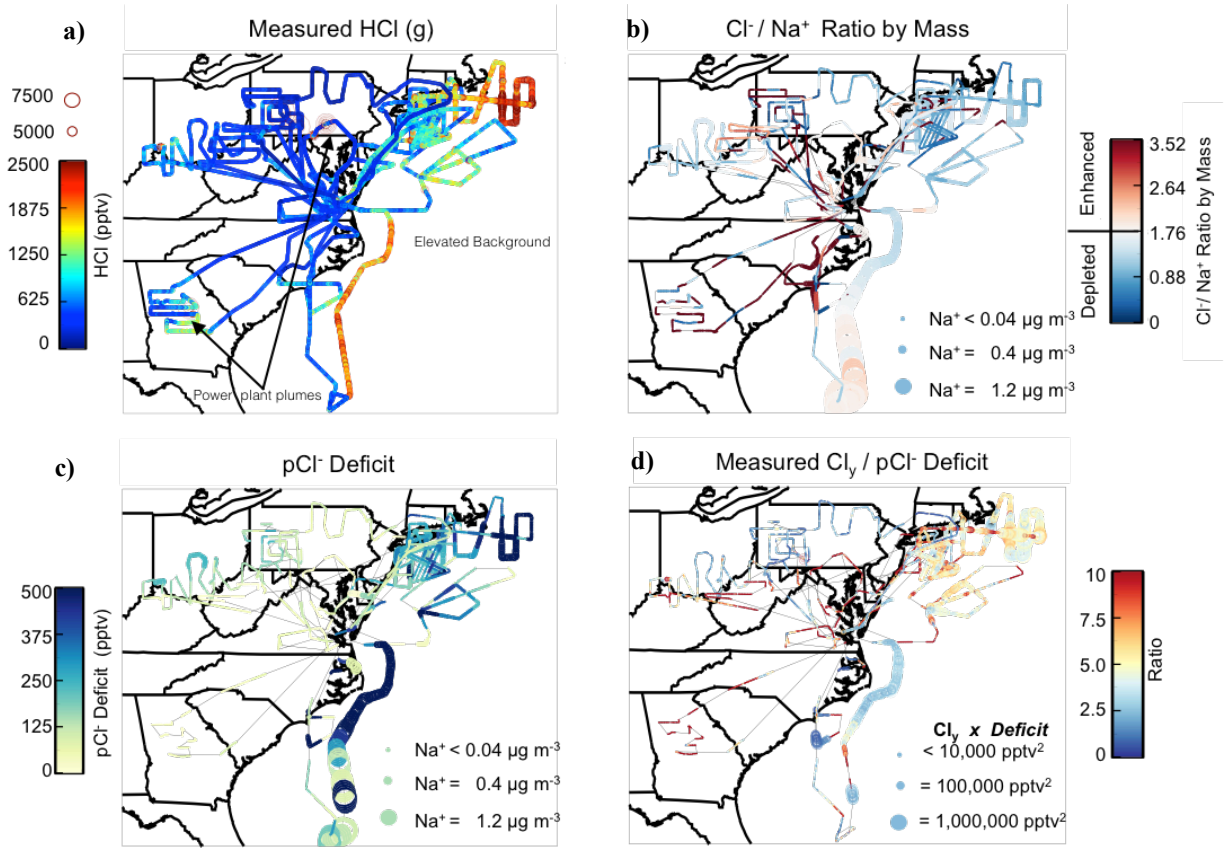

Figure 5: a) Maps showing the 10s measurements of HCl from CIMS colored by total concentration with points sized by the multiplicity by which they exceed the maximum of the color scale **b)** The ratio of the UNH Cl^- to the UNH Na^+ (D_p <4 µm) measurements by mass as compared to the sea-water ratio, sized by absolute sodium concentration **c)** Particle chloride deficit calculated by taking UNH filter measurements of sodium multiplied by the seawater ratio of Cl- to Na+ and subtracting the amount of UNH filter measurements of chloride, sized by absolute sodium concentration **d)** The total of HCl and $ClNO_2$ measured divided by the calculated chloride deficit (approximately the quotient of panel A and panel C), and sized by the product of total Cl_y and the calculated chloride deficit. Large points indicate where large Cl_y is collocated with a large chloride deficit, while color indicates the magnitude of their ratio.

between the product of measured sodium and the seawater ratio of Cl^-/ Na^+ and the measured particle chloride. The chloride deficit, then, gives the concentration of chlorine that has been removed from the particle. Comparing Panel A and C, it can again be seen that the areas where the highest HCl concentrations are those where chloride deficit is large suggesting that some of the elevated HCl concentrations can be attributed to the equilibrium partitioning of particle chloride out to the gas phase.

By taking the ratio of the total gas phase chlorine species to the amount of displaced particle chloride, it can be determined if the elevated levels of gas phase species over the ocean can be explained by the displaced chloride from oceanic particles, which is shown in Panel D in **Figure 5.** However, as the figure shows, the amount of chloride displaced from the particle is almost never enough to explain the full concentrations of HCl (g) that were observed during the WINTER campaign (i.e. the ratio is almost never less than or equal to one). Typically, the ratio of the total measured HCl (g) and $ClNO_2$ (g) is 2-7 times larger than the amount of chloride that is displaced from the particle with respect to sodium in areas where both the measured Cl_y and pCl^- deficit are large (i.e. point sizes on Panel D) indicating that there is more mass of gas phase chlorine species than can be explained by the measured amount of displaced particle chloride. Even if only HCl, instead of total gas phase Cl_y is compared to the amount of displaced particle chloride, the total amount of measured gas phase HCl is still >2x larger than the amount of displaced chloride relative to sodium. Furthermore, uncertainty in Cl_y gas phase measurements is not enough to explain the discrepancy (see **Figure 6**).

There are several possible explanations for this discrepancy. If the lifetime against deposition of sodium in the aerosol is shorter than the lifetime of HCl, then some of the HCl mass could be explained as residual from displaced chloride aerosol that has already been

removed from the atmosphere. Furthermore, many of the areas sampled over the ocean with elevated HCl concentrations were downwind of major populated areas where power-plant emissions of HCl could have been advected downwind that would enhance Cl_y emissions relative to particle sodium concentrations thereby increasing the ratio greater than what it would be if displacement of chloride is considered to be the only source.

The atmospheric lifetime of HCl is primarily controlled by wet and dry deposition. The dry deposition velocity of HCl in marine environments has been estimated to range between 1 and 5 cm s^{-1} [Finlayson-Pitts and Pitts, 1999]. In the observed aerosols during the WINTER campaign, pH is so low that equilibrium partitioning of HCl into the particle is negligible since HCl is displaced under the vast majority of conditions making wet deposition unlikely. At deposition rate of 1 cm s^{-1}, the lifetime against deposition is 1.2 and 1.7 days at a boundary layer height of 1 km and 1.5 km, respectively. The 24 hour averaged lifetime of HCl with respect to OH oxidation of 15 days (k_{OH+HCl} (298 K) = 8×10^{-13} cm^3 $molecule^{-1}$ s^{-1} and $[OH]_{24\,h} = 1 \times 10^6$ molecules cm^3). However lower OH levels in winter, this lifetime against OH oxidation is likely even longer, making dry deposition the primary removal mechanism of HCl from the troposphere. As previously noted, super-micron sea salt aerosols have a relatively short lifetime against deposition (~1.5 days) [Erikson et al., 1999; Keene et al., 1999] comparable to that of HCl against dry deposition while submicron sea-salt has a lifetime of ~1-2 weeks. The UNH filter measures both super-micron and submicron sea-salt aerosols with $D_p < 4$ μm. Since most of the sea-salt mass is associated with super-micron particles it is likely that the mean lifetime of aerosols sampled by the UNH filter is on the shorter end. Therefore, it is not unreasonable to assume that some of the HCl measured could have been from displaced particle chloride whose

aerosol had since been deposited, since HCl was measured in significant quantities at both 1km and 1.5km, where HCl would have a slightly longer lifetime than super-micron sea-salt aerosols. However, because most of the chloride mass would be expected to be in larger particles (D_p> 4 μm) that the UNH filters may or may not have measured, the discrepancy in the chloride deficit and available chloride measured shown in **Figure 5** could also be explained by some unmeasured fraction of coarse mode sea salt.

As noted, the areas in which Cl_y observations are elevated and largely unexplained by the amount of displaced chloride from the particle do coincide with areas downwind of major population centers with coal burning power-plants, potentially significant wood-burning sources, and widespread road salting habits during the winter. **Figure 6** shows the total Cl_y, chloride

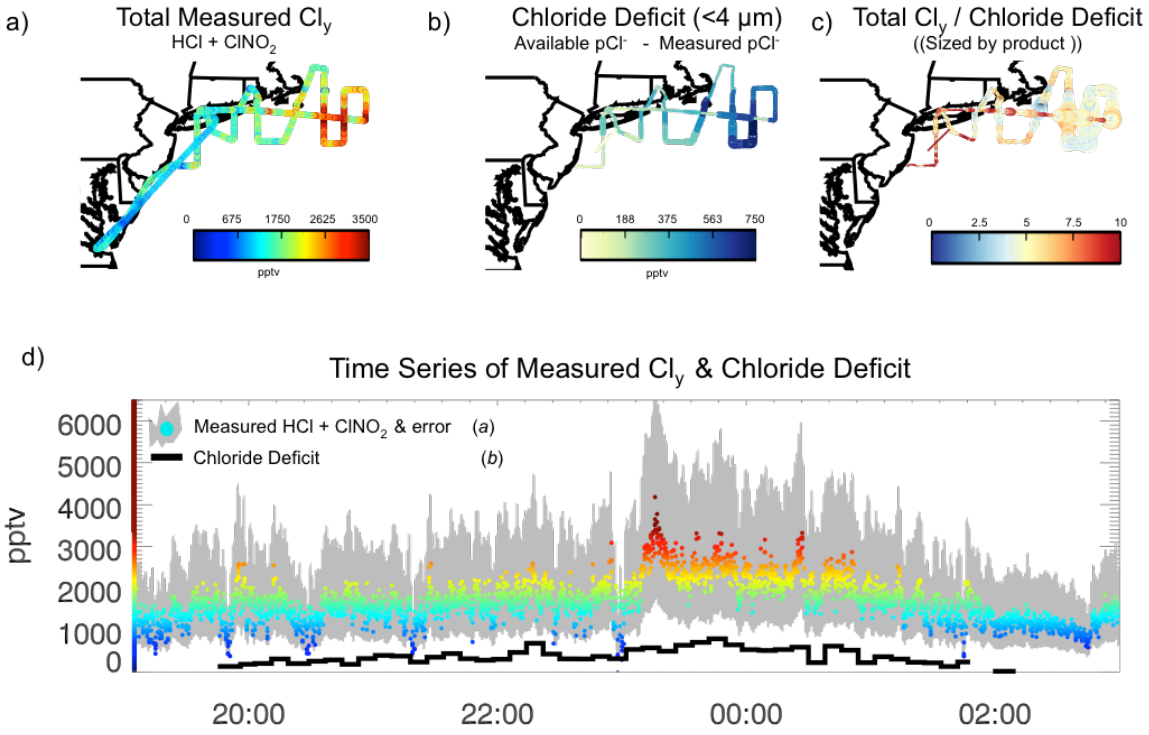

Figure 6: Maps showing the total measured Cl_y (**a**), chloride deficit (**b**), and their ratio (**c**), as defined above, during Research Flight 3 on the night of 02/07/15 and (**d**) a time series of the deficit in black and measured Cl_y in color, on the same color scale as panel **A** for comparison, with the estimated measurement error shaded in grey

deficit and their ratio both spatially and as a time series for Research Flight #3 which saw some of the highest Cl_y concentrations, submicron chloride concentrations, and chloride deficits throughout the campaign. In this flight, $HCl+ClNO_2$ reached sustained concentrations> 1800pptv with a maximum 4866 pptv where displacement from the particle is only 573 pptv leading to a ratio of Cl_y : Deficit equal to ~8.5, leaving 4293 pptv to be explained by some combination of other anthropogenic sources of HCl and residual HCl from previous displacement where aerosols have since been deposited. While that is a very significant amount of unexplained HCl, the median for this flight is 1685 pptv of Cl_y, with a median chloride deficit of 313pptv, leaving 1372 pptv of Cl_y unexplained by displacement of chloride from the particle. Panel D shows that the uncertainty in the Cl_y measurements, shaded in grey, cannot explain the difference in the measured chloride deficit and Cl_y, observations indicating that this feature of either residual HCl and/or additional downwind sources of HCl are statistically significant.

It is of note that a median of 313 pptv HCl displaced from the particle for this flight is not an insignificant amount. In pristine areas of the marine boundary layer where anthropogenic contributions are minimal, chloride displacement from the particle is the largest source of lower tropospheric HCl [Keene et al., 1999]. Models, which do not incorporate aerosol thermodynamics, cannot reproduce this partitioning of particle chloride into gas phase HCl and its sensitivity to atmospheric composition, motivating a need for validating ISORROPIA II's ability to do so accurately.

4.2 Observed & ISORROPIA II Chlorine Partitioning

The median observed mass fraction of chlorine in the fine mode particle phase (pCl^-), determined using the AMS measurements, is 0.054 ($Q_{25\%} = 0.038$, $Q_{75\%} = 0.084$) for the whole campaign, with large variability about this average. The observed pCl^- varies across a range of 0-

20%, even within a single flight, presumably driven by changes in particle liquid water content and pH. Panel A in **Figure 7** shows the measured fraction of bulk chlorine in the particulate (AMS pCl^- / [AMS pCl^- + CIMS HCl]) as a function of ISORROPIA II predicted pH from the *Base+ Cl* simulation, that is colored by observed relative humidity. Each point in **Figure 7** has a different bulk aerosol composition (both in mass and relative contributions from various anions and cations) and different activity coefficients, thus they would not be expected to line up along a single function.

As **Figure 8** shows, although the model captures the observed nitrate-partitioning well, it tends to significantly overestimate the amount of chloride in the particle and, therefore underestimate the amount of HCl in the gas phase by a factor of 2.14 on average. The nitrate partitioning results shown here are not significantly different than those presented in Guo et al., 2016, indicating that the pH perturbation caused by added reactive chloride is not enough to perturb the nitrate partitioning, which will be discussed further below in section 4.4. The model predicted results in **Figure 7B** show the model-measurement disagreement in chlorine partitioning further. The model predictions follow an exponential relationship with pH, as expected, and that the observations in **Figure 7 A** also somewhat follow, but at a lower magnitude with scatter driven by variations in composition and environmental conditions for a given predicted pH. The model results in **Figure 7 B** predict there to be a considerably larger fraction of chloride in the particle than the observations show even at high relative humidities. At extremely low pHs (< 0.25), the scatter and divergence in the observations (**7A**) from the ideal modeled behavior (**7B**) increases. he model predicts that no aqueous chloride can exist in the particle at pH< 0, but observations show that the particle very rarely is completely depleted

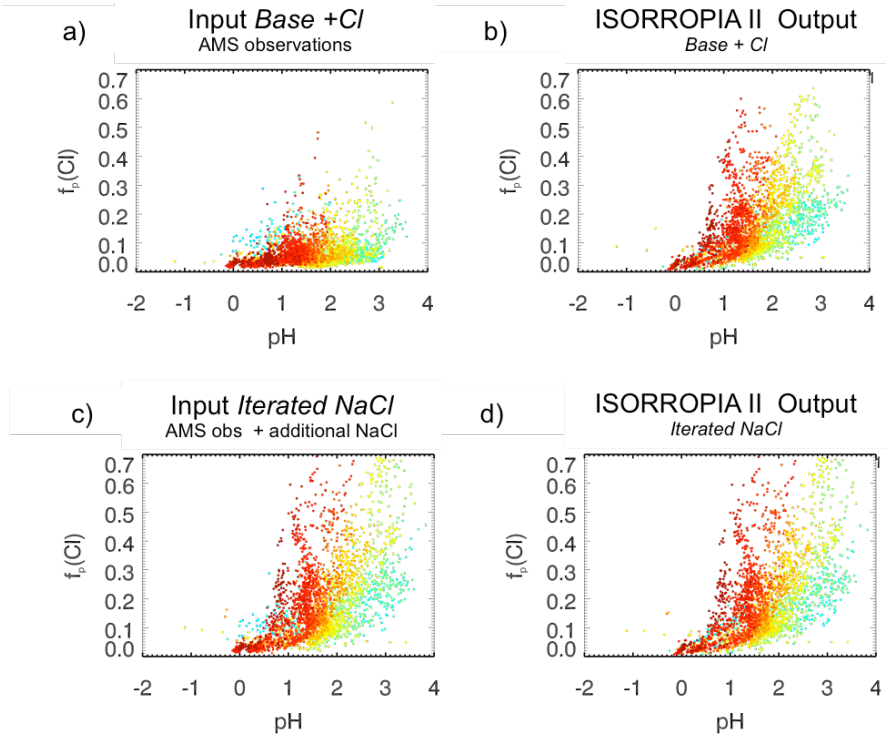

Figure 7: Figure comparing the observed chlorine partitioning and the model predicted chlorine partitioning **a)** the observed fraction of chloride in the particle as a function of model predicted pH and colored by relative humidity from the *Base + Cl* original ISORROPIA II simulation**. b)** The model predicted partitioning for the *Base +Cl* simulation. **c)** Input fraction of chloride in the particle as a function of pH once particle sodium chloride has been iterated to match the observed HCl concentrations from the *iterated NaCl* ISORROPIA II simulation**. d)** The output of the *iterated NaCl* simulation ,which by experimental design matches the input.

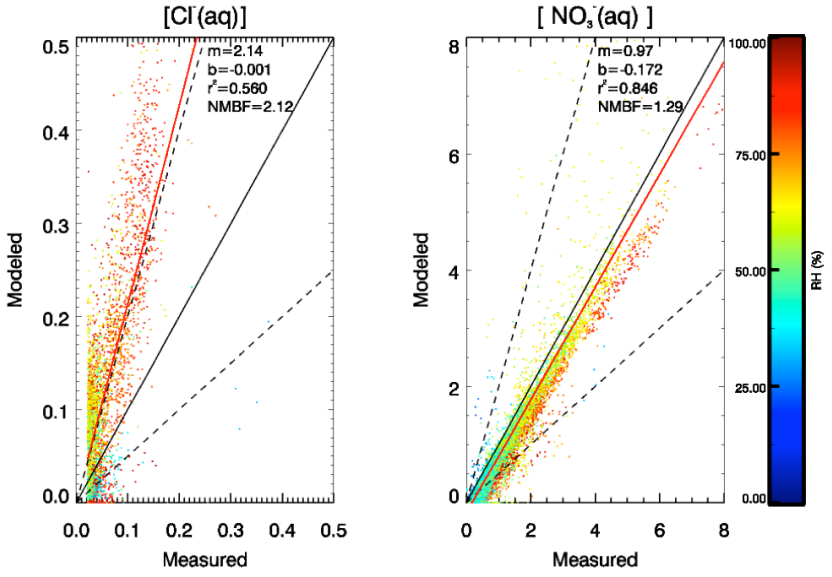

Figure 8: Figure comparing the observed chlorine partitioning and the model predicted chlorine partitioning a) the observed fraction of chloride in the particle as a function of model predicted pH and colored by relative humidity from the Base + Cl original ISORROPIA II simulation. b) Same figure showing model-measurement agreement of the nitrate partitioning

in aqueous chloride, even at these low predicted pH values. The predicted pH for these points is either too low or there is some limiting process that prevents the particle from ever becoming totally depleted in chloride.

It is possible that the original model-measurement disagreement results in the *Base+ Cl* simulation because the total soluble chloride provided as input to ISORROPIA II did not include contributions from submicron sea-salt since the AMS does not measure sea-salt in its particle chloride measurement. This possibility is the reason that the second simulation included an iteration of the aqueous sodium and chloride until the predicted gas phase HCl matched that of the observations.

Panel C and D in **Figure 7** show the input and output to ISORROPIA II that result from the *Iterated NaCl* simulation where sodium chloride was added as input until the predicted HCl matched the observations. By experimental design for this simulation, the input partitioning matches the outputted partitioning. It should be noted that the output from the model between the *Base+ Cl* simulation (**7B)** and the output from the *Iterated NaCl* simulation (**7D**) are not significantly different. This is noteworthy because it means that the amount of sodium chloride added in the *iterated NaCl* simulation did not significantly perturb the predicted chlorine partitioning. The difference in **Figure 7**, panel A and panel C shows that the input to the model was changed between the two simulations, but that the outputted partitioning did not change since the amount of added sodium chloride was not large enough to perturb pH in a way that would change the chlorine partitioning. The reason for this will be discussed further in section 4.4.

Figure 9 shows a series of example time series taken from Research Flight 3 off the coast of New York City on the night of 02/07/15. **Panel 9A** shows the Base + Cl simulation's

predicted and observed chlorine partitioning. Here, ISORROPIA II's consistent bias in over predicting the concentration of particulate chloride is seen. With a slope of 2.14, the model predicts nearly twice the amount of chloride should be in the particle than is measured. The cases where ISORROPIA II over estimates the measurements the most tend to be co-located with points where the relative humidity is high (likely driven by a decrease in temperature at a constant pressure). The measurement uncertainty in the AMS particle chloride measurement is shaded in grey around the observation. Shaded around the model predicted aqueous chloride concentrations is the variation in the model output calculated from the upper and lower limits of

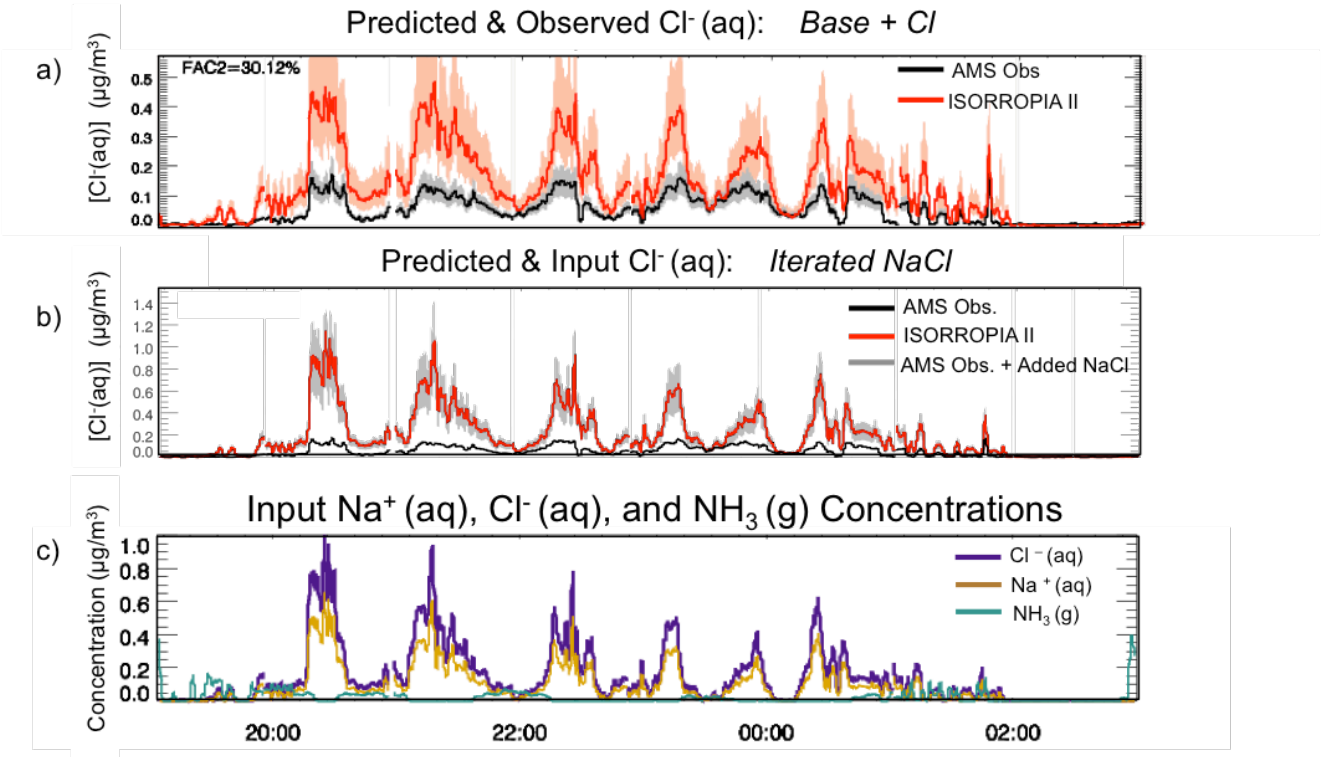

Figure 9: Time series taken from Research Flight 3 off the coast of New York City on the night of 02/07/15. **a)** The *Base + Cl* predicted aqueous chloride concentrations from ISORROPIA II compared to the AMS observations with measurement uncertainty and model response to measurement uncertainty shaded. **b)** The *Iterated NaCl* predicted aqueous chloride concentrations from ISORROPIA II compared to the inputted chloride observations that include added NaCl with the measurement uncertainty of the AMS shaded. **c)** Time series showing the total amount of aqueous chloride and sodium, and NH_3(g) that must be added bring the model-measurement gas-particle chlorine partitioning into agreement.

the HCl measurement uncertainty. It is clear from this time series that the uncertainty in the particle chloride and HCl measurements is not enough to explain the model-measurement discrepancy observed in the gas-particle partitioning of chloride since the shaded areas of the model sensitivity to measurement uncertainty and the measurement uncertainty being compared to never overlap.

For this specific flight, only 30.1% of model outputted aqueous chloride was within a factor of 2 of the measurements in the *Base+ Cl^-* simulation. For this base simulation, the nitrate partitioning showed model agreement always within the measurement uncertainty. **Panel 9B** shows the same time series for the same flight for the *Iterated NaCl* simulation. By design, now 100% of points fall within a factor of 2 of the inputs. **Panel 9C** shows the amount of particle chloride, sodium, and ammonia that must be added in order for the model to simultaneously match the gas phase HCl and particle NH_4 measurements. This specific flight required the most particulate chloride and sodium to be added in order to match the observed HCl measurements, but was also the flight where HCl measurements were the largest over the ocean (see **Figure 5A**). Presumably, in order to sustain such high levels of HCl in the gas phase, a substantial amount of particulate chloride needed to be present to produce & account for the large amount displaced to the gas phase. For this flight, the areas where the most sodium and chloride needed to be added to the particle to account for the missing sea salt contributions correspond to those where the other particle mass concentrations are elevated. **Figure 7** highlights the fact that adding small amounts of submicron sodium chloride does not significantly perturb the predicted chlorine partitioning (i.e. why the model predicted response in panel B and panel D look so similar), but that change in inputted chlorine is enough to bring the inputs into agreement with the predicted output. Although in some cases for this flight, the amount of particle chloride that

is needed to explain the amount of HCl in the gas phase is nearly twice or three times the amount that is measured, **Figure 7** shows that this is not enough to perturb the original predicted partitioning, regardless. So while it represents a substantial change in the amount of submicron chloride that is predicted, it does not necessarily have as significant of an effect on the aerosol

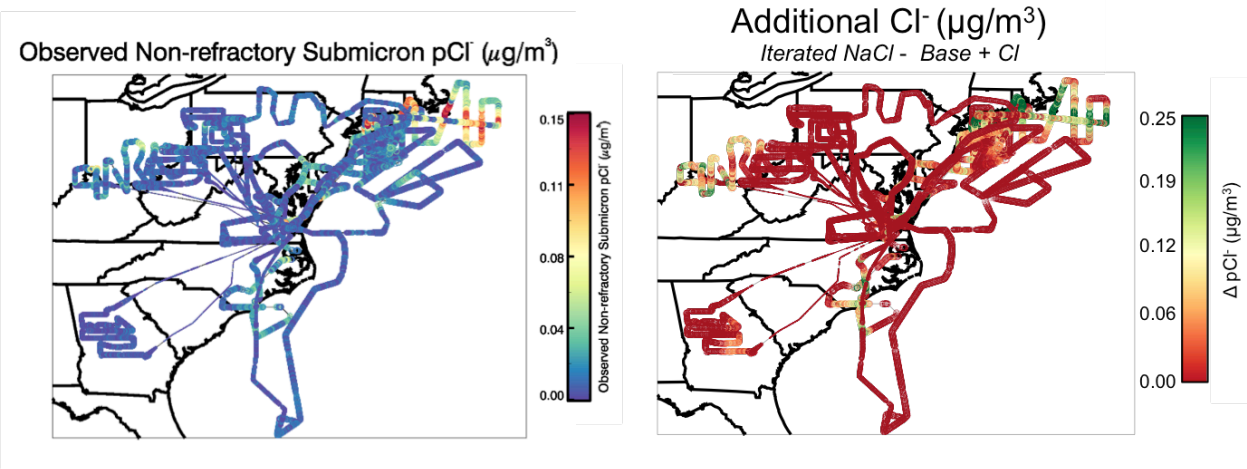

Figure 10: Map of the observed submicron non-refractory particle chloride observed by the AMS (a) and the amount of additional particle chloride that must be added to get the modeled gas-particle partitioning to match the observed gas phase HCl measurements (b).

thermodynamics that ultimately affect chlorine, nitrate, and other compounds partitioning between the gas and particle.

Figure 10 shows a map of the observed particulate chloride as measured by the AMS (a) and the amount of additional chloride (and sodium) that was added in the iterated NaCl simulation to bring the model's predicted gas phase HCl into agreement with the measured HCl(g) for all flights. **Panel 10B** highlights where Research Flight 3, off the coast of New York, required a significant fraction of submicron sodium chloride to be added to bring the model into agreement with the measurements. The inland areas where significant amounts of submicron sodium chloride was required to be added correspond to areas where the inland HCl(g) was elevated presumably due to emission from power plants. For reference, the detection limit of the

PILS instrument capable of measuring chloride was 0.2 μg/m^3. As **Figure 10** demonstrates, the amount of additional sodium chloride needed to explain the model-measurement disagreement in gas-particle chloride partitioning is less than what the PILS detection limit for nearly all of the flights during the WINTER campaign. Therefore, the amount of refractory chloride needed to explain the model-measurement disagreement is not inconsistent with the observations.

4.4 Controls on the Phase Partitioning of Bulk Chlorine

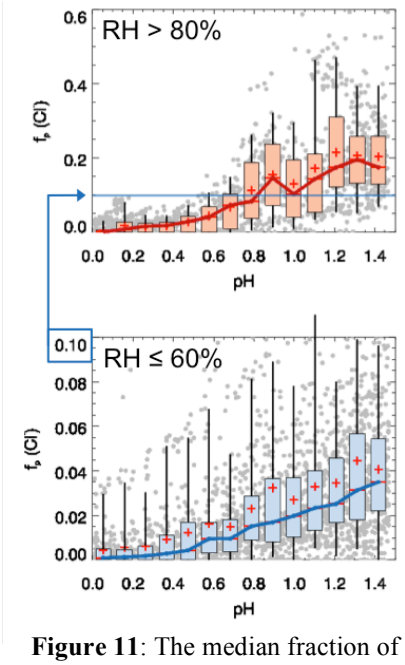

Figure 11: The median fraction of chloride in the particle as a function of pH subdivided into different relative humidity regimes as predicted by ISORROPIA for the *iterated NaCl* simulation

Aerosol liquid water content, pH, and temperature are understood to be strong levers on gas-particle equilibrium partitioning. During the WINTER campaign, only in very humid conditions (RH >80%) was any substantial amount of total partitionable chloride predicted by ISORROPIA II in the iterated sodium chloride simulation to be present in the particle (~20 - 40%) as shown in **Figure 11** This figure is just a summary of the information contained in **Figure 7B,** zoomed in on a smaller pH range**.** Upon looking at time series of the partitioning of bulk chlorine to the particle and that of various predictive variables, it was found that liquid water content could explain the most variance in the amount of measured chloride in the particulate. This confirms the expectation that under wetter conditions, more chloride can partition into the particle. Ultimately, the validity of the assumption that the aerosol in question is deliquesced and therefore able to participate in heterogeneous chemistry is key in determining whether ISORROPOIA II has skill at reproducing the measured gas-particle partitioning of chlorine. What is evident in **Figure 11** is just how steep

the predicted partitioning of chlorine is in pH space, specifically at high relative humidities. Even a slight pH perturbation (~0.1 units) to particles with pH > 0.8 can lead to significant enough changes in the aqueous particle chloride concentration (> 0.20 ug/m^3) to sustain heterogeneous halogen chemistry and its many downstream impacts. At lower pH values <0.8, all of the partitionable chloride is thought to be in the gas phase, so slight perturbations do not affect its partitioning significantly. This also the case when relative humidity is <60%, where, because so little chloride exists in the particle already, slight pH changes even at pH 1.5 - 2 do not substantially impact the absolute concentration of aqueous chloride.

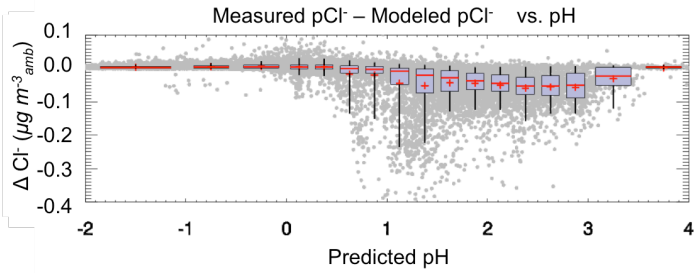

Figure 12: Scatter plot of the Base+ Cl simulation aqueous chloride model to measurement agreement as a function of predicted pH. Box and whisker plots showing the mean, median, and range of the ratio of agreement are also shown for different bins of predicted particle pH.

Figure 12 shows aqueous chloride was generally over predicted in the *Base + Cl* simulation when pH >0.8. Below pH of 0.8, so little aqueous chloride is in the particle that any absolute error is small. Similarly, above pH=2, the error is smaller since the predicted partitioning has more of the total chlorine in the gas phase. Ultimately, the largest model errors occur at high relative humidities in the pH range 0.8-2 during WINTER, as these conditions are where chloride partitioning is most sensitive. Particle liquid water content and particle pH are inherently connected. Throughout this work, we have addressed potential assumptions that could either systematically bias pH or liquid water content. In theory, by altering particle sodium chloride concentrations in the *iterated NaCl* simulation, we are changing aerosol pH and therefore moving up and down the predicted partitioning line. However, ISORROPIA II does not

always explicitly calculate pH based on all of the components it is given. It first calculates the total sulfate ratio (R_1), which is defined in as:

$$R_1 = \frac{[NH_4^+] + [Ca^{2+}] + [K^+] + [Mg^{2+}] + [Na^+]}{[SO_4^{-2}]}$$

During the WINTER campaign, this ratio is set only by the total ammonia, sodium, and sulfate. For sulfate rich cases (R1< 2), $NH_3(g)$, $NO_3^-(aq)$ and $Cl^-(aq)$ are assumed minor species that do NOT significantly perturb the equilibrium through the following reactions:

$$NH_3(g) + H_2O(aq) \longleftrightarrow NH_4^+(aq) + OH^-(aq)$$
$$HNO_3(g) \longleftrightarrow H^+(aq) + NO_3^-(aq)$$
$$HCl(g) \longleftrightarrow H^+(aq) + Cl^-(aq)$$

The model then solves the appropriate set of equilibrium reactions (for the major species) and the three gases $NH_3(g)$, $HNO_3(g)$, $HCl(g)$ are subsequently dissolved through the equilibria described above. The same is assumed for the dissolved undissociated ammonia, nitric and hydrochloric acid in the aqueous phase ($NH_3(aq)$, $HNO_3(aq)$, $HCl(aq)$). Thus, sulfate poor cases, where R_1>2, are the only regimes in which the pH is allowed to be perturbed by the iterated sodium chloride or NH_3 concentrations. This treatment of when to allow minor species to affect particle pH is a fair assessment, since in sulfate rich cases, particle pH is so low because of the amount of sulfate that all of the nitrate and chloride are presumably in the gas phase and all of the ammonium is in the particle. Simply, when it is in a sulfate rich regime, the pH is so low that the partitioning of nitrate, chloride, and ammonium is not sensitive. **Figure 13** shows a map of what the total sulfate ratio was determined to be during the WINTER campaign. **Panel 13A** shows that about half of the area sampled during the campaign was in the sulfate rich regime where particle pH is unaffected by sodium chloride. Those areas correspond to areas where the pH is <1 in **panel 13B**, and in **panel 13C**, where the pH does not change by iterating sodium chloride. In the sulfate poor areas, the original predicted pH tends to be higher, and is the only

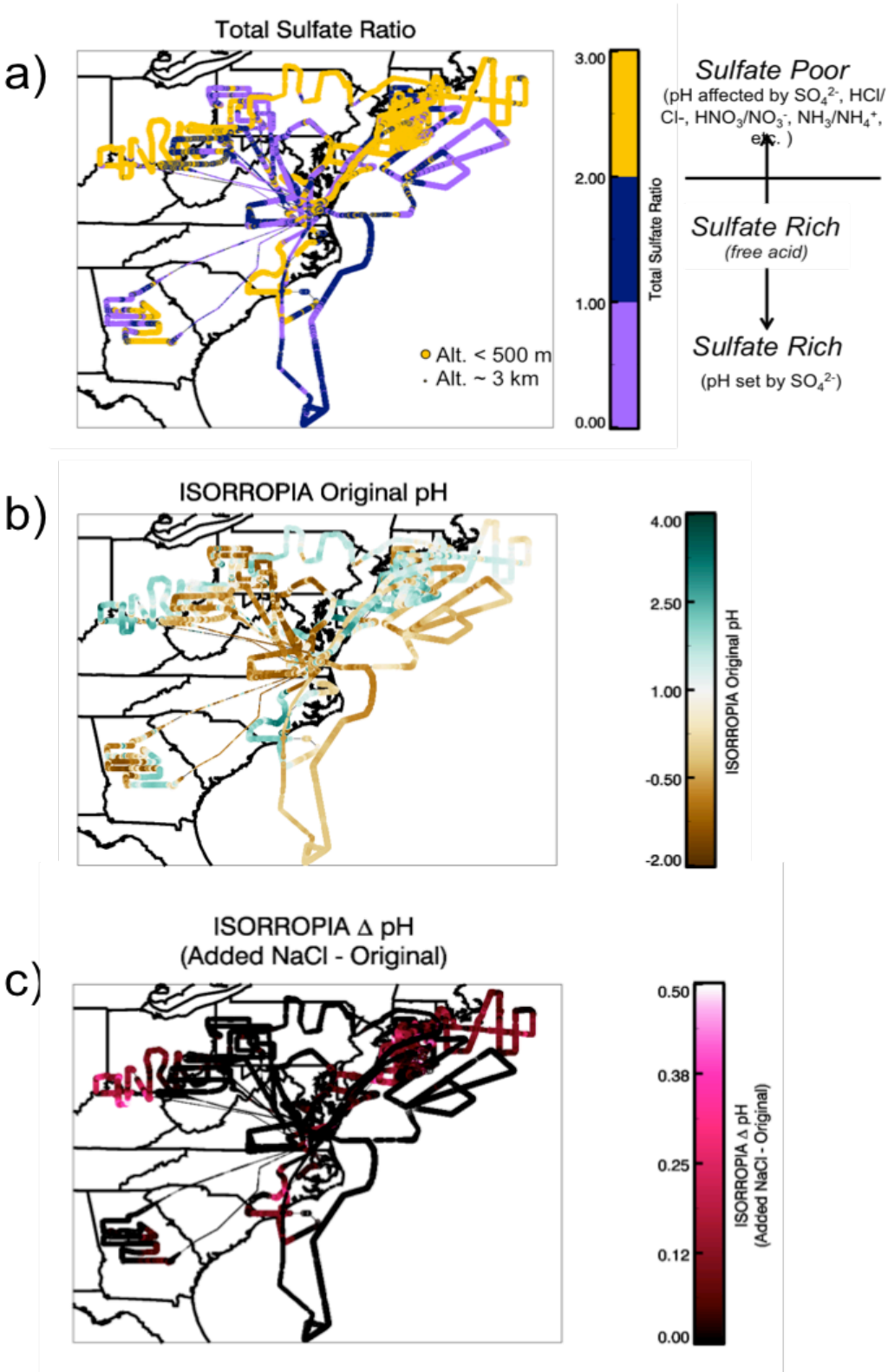

Figure 13: **a)** the total sulfate ratio during the WINTER campaign, **b)** the predicted ISORROPIA II pH for the *Base + Cl* simulation and **c)** the change in pH from adding sodium chloride in the *iterated NaCl* simulation

area where pH does change by iterating sodium chloride. **Figure 7** demonstrated that the model predicted chlorine partitioning does not shift after iterating sodium chloride concentrations showing the model's insensitivity to the changes in input total chloride that were made in the *iterated NaCl* simulations. **Figure 13** shows that the model is largely insensitive to total chloride inputs because nearly half of the area sampled during the campaign was in the sulfate rich regime where particle pH is unaffected by sodium chloride since it is already low. Therefore, for much of the WINTER campaign, the input changes made in the *Iterated NaCl* simulation were not allowed to affect partitioning because of the way ISORROPIA II solves equilibrium. In the few cases where particle pH was affected, as in the Research Flight # 3 case study presented in **Figure 9**, the median pH change from adding sodium chloride is only 0.10 units, but as we saw in **Figure 7**, this is all that is necessary at the high relative humidity that was observed during the flight to significantly change the observed gas-particle chlorine partitioning since the partitioning curve for HCl is so steep in pH space in the pH range relevant for the WINTER campaign. From the iterated NaCl simulations, and estimate of how much sodium chloride was present in submicron particles that the AMS did not detect is obtained.

5 DISCUSSION

Inconsistencies between observed and modeled gas-particle partitioning of any species using ISORROPIA II can reflect (1) observational input violating inherent assumptions of the model, (2) observational uncertainty in bulk measurement input, (3) errors in thermodynamic constants used in the model, or (4) errors from numerical methods used to solve equilibrium equations. It is important to understand these potential causes of disagreement to extract meaningful results from the ISORROPIA II results presented above. An examination of some

possible reasons for the disagreements between ISORROPIA II predictions and WINTER chlorine partitioning are discussed below.

In section 3.2, it is noted that ISORROPIA II is run in "metastable" mode, which assumes the aerosol remain deliquesced regardless of relative humidity. Model to measurement disagreement was greatest in chlorine partitioning when the relative humidity was between 30-65% could be due to assumptions about particle phase state. The deliquescence relative humidity of pure NaCl is around 68%, which can be lower in the presence of other salts. Freshly released sea salt aerosols are usually already deliquesced making their efflorescence behavior of more relevance. Recent studies have shown that mixed NaCl and $NaNO_3$ based salts have a mutual efflorescence relative humidity around 30% [Gupta et al., 2015. Marine air masses sampled with ambient relative humidity in between the efflorescence and deliquesce relative humidifies could either be crystalline or aqueous solutions depending on the relative humidity history of the air mass. If particles are assumed to be deliquesced, but were in fact effloresced because they had recently passed through an air mass dry enough to completely effloresce the particle, the sample particle chloride would be unable to partition to the gas phase such that partitioning would not be in equilibrium. While this is a difficult assumption to asses without running back trajectories on every air mass sampled during the campaign, relative humidity and the relevant ambient conditions needed to predict whether a particle within the variable phase range are tracked in global models such that this assumption could be easily tested before deciding whether to allow the equilibrium partitioning of bulk chloride. Ultimately, while this assumption may be the cause of some disagreement in the results presented here, it would not be as difficult in using ISORROPIA II to predict heterogeneous chlorine partitioning in a coupled global model since cases in which the particle may have effloresced could be identified.

ISORROPIA assumes that the bulk properties passed as input represent the overall particle composition such that pH (and therefore partitioning) does not vary with particle size. When sampled in bulk, compounds with pH-dependent solubilities such as HCl, HNO_3, and NH_4 are not always representative of the real atmosphere since the pH of the bulk may diverge significantly from that of the size fractions with which individual gas preferentially partition (Young et al., 2013). In marine air, like much of that sampled in the WINTER 2015 aircraft campaign, particulate Cl^- and NO_3^- are typically associated with supermicrometer size fractions whereas most NH_4^+ is associated with submicrometer size fractions because on average, larger marine aerosol size fractions are less acidic than smaller size fractions. We assume that particles are internally mixed across the submicrometer portion of the size distribution. This assumption is difficult to test without size resolved composition measurements below 1 μm, which were lacking during the WINTER campaign. As such, some of the disagreements between predicted and observed chloride partitioning may have resulted from fresh submicron sea spray emissions occurring into the submicron mode leading to a steady state externally mixed portion of particle chloride mass.

The gas-particle equilibrium of a system is governed by the chemical potentials of the components, which in turn depend upon the ionic composition of the solution and the activity coefficients of the solute and solvent. These properties are affected by environmental conditions such as temperature and relative humidity, which sets water activity and thus component concentrations and the maximum possible relative humidity at which a solid species can exist, known as the deliquescence relative humidity. However, since the advent of gas-particle equilibrium models, both the numerical methods used to solve these sets of equations and the constants assumed have been debated. Kim et al., 1993 and subsequent comparisons of

ISORROPIA II to more explicit equilibrium models, like E-AIM, have pointed out the inconsistencies that can arise by using different methods to estimate water activity coefficients and solute activity coefficients, as well as the effect of ignoring charge balance on pH.

a)

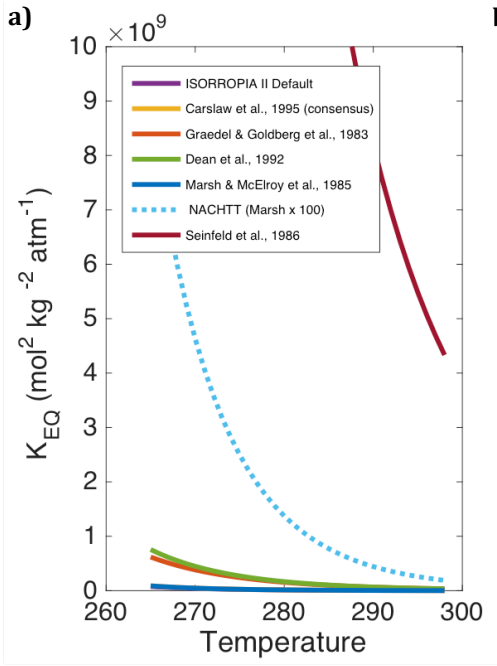

b)

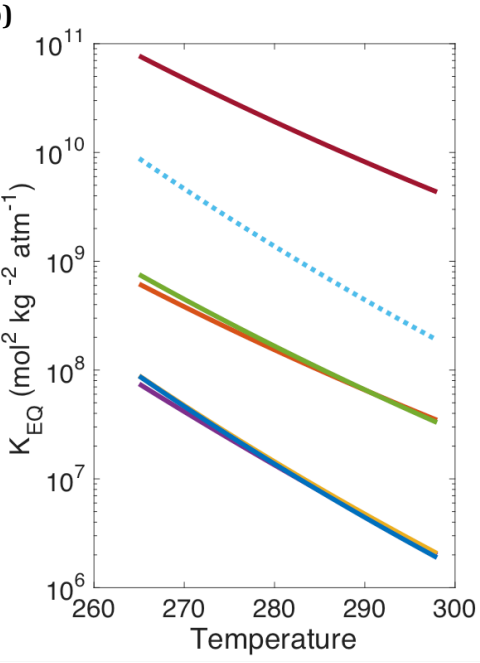

c)

	K_H (mol • kg^{-1} atm^{-1})	K_A (mol • kg^{-1})	K_{EQ} (mol^2 • kg^{-2} atm^{-1})	Note
Carslaw et al. (1995), Wagman et al. (1982), Brimblecombe & Clegg (1989)	--	--	$2.0326 \times 10^6 \exp\left[9000\left(\frac{1}{T}-\frac{1}{T_0}\right)\right]$	All are thermodynamic calculations based off Wagman et al., 1982. Data collected in 1963
Graedel & Goldberg (1983) *	20.3260	$1.7051 \times 10^6 \exp\left[6896\left(\frac{1}{T}-\frac{1}{T_0}\right)\right]$	$3.4658 \times 10^7 \exp\left[6896\left(\frac{1}{T}-\frac{1}{T_0}\right)\right]$	Based on data taken from Nemeth et al., 1975 , for which source couldn't be obtained
Dean (1992)*	$19.3097 \exp\left[600\left(\frac{1}{T}-\frac{1}{T_0}\right)\right]$	$1.7051 \times 10^6 \exp\left[6896\left(\frac{1}{T}-\frac{1}{T_0}\right)\right]$	$3.2925 \times 10^7 \exp\left[7496\left(\frac{1}{T}-\frac{1}{T_0}\right)\right]$	Only the tabulated data between T = 273K and T = 303K from Dean (1992) were used to derive H and its temperature dependence.
Marsh & McElroy (1985)	$1.1033 \exp\left[2300\left(\frac{1}{T}-\frac{1}{T_0}\right)\right]$	$1.7051 \times 10^6 \exp\left[6896\left(\frac{1}{T}-\frac{1}{T_0}\right)\right]$	$1.881 \times 10^6 \exp\left[9196\left(\frac{1}{T}-\frac{1}{T_0}\right)\right]$	Thermodynamic calculations based on data in West & Hull, 1933, and Harned & Owen 1958 . Valid for $0 < T\,^{\circ}C < 50$, $2 <$ wt % < 36
Young et al. (2013) – NACHTT *	$110.33 \exp\left[2300\left(\frac{1}{T}-\frac{1}{T_0}\right)\right]$	$1.7051 \times 10^6 \exp\left[6896\left(\frac{1}{T}-\frac{1}{T_0}\right)\right]$	$1.881 \times 10^8 \exp\left[9196\left(\frac{1}{T}-\frac{1}{T_0}\right)\right]$	Found that increasing the Marsh & McElroy et al., 1985 Henry's Law by 2 orders of magnitude matched observations
Seinfeld (1986) *	2.5407×10^3	$1.7051 \times 10^6 \exp\left[6896\left(\frac{1}{T}-\frac{1}{T_0}\right)\right]$	$4.2708 \times 10^9 \exp\left[6896\left(\frac{1}{T}-\frac{1}{T_0}\right)\right]$	Taken from old textbook, for which most updated version quotes the Marsh & McElroy 1985 value for K_H . Lit review states how original value was obtained is not clearly stated
ISORROPIA II K_{EQ}	--	--	$1.971 \times 10^6 \exp\left[30.20\left(\frac{T_0}{T}-1\right)+19.910\left(1+\ln\left(\frac{T_0}{T}\right)-\frac{T_0}{T}\right)\right]$	Based of Wagman et al., 1982

Figure 14: **a)** Figure showing the temperature dependency of the various published values for the effective equilibrium constant **b)** Same figure, in log space **c)** Table showing the functions used to calculate panel A and B.

*Denotes that effective equilibrium constant quoted uses the acid dissociation function that is derived in Marsh & McElroy (1985).

Specifically, in the case of HCl, there is more than 3 orders of magnitude spread in the published values of basic thermodynamic properties like the value of the Henry's law constant at room temperature and a spread of a factor of 1.5 in the temperature dependency of the Henry's law constant used to calculate the equilibrium constant for chlorine partitioning [Sander et al., 2015]. constant and acid dissociation constant) compared to the default value of ISORROPIA II. While there are several different values of the Henry's Law constant for HCl in the published literature, only one value was found for the acid dissociation constant of HCl from Marsh & McElroy, 1985, based on data taken in the '60s. Because ISORROPIA II only uses an effective equilibrium constant, the single acid dissociation constant from Marsh & McElroy, 1985 was used to calculate effective equilibrium constants from published physical Henry's Law constants in order to make a comparison to possible values ISORROPIA II could use.

The published values of effective equilibrium constants range across several orders of magnitude with slightly different temperature dependency values. However, quoting only the range of these values is somewhat misleading. The highest value of the Henry's Law constant, published in Seinfeld, 1986 textbook, has since been updated in more recent editions to be the value quoted in Marsh & McElroy, 1985. As pointed out in a recent literature review of Henry's Law constants [Sander et al., 2015], the basis for the value in Seinfeld, 1986 was not clearly stated in the original work. Young et al., 2013 uses the absolute range of Henry's law constants shown in the table above to justify multiplying the Henry's Law constant of Marsh & McElroy, 1985 by 100 in order to bring the E-AIM modeled chlorine partitioning into agreement with their observed chlorine partitioning, stating that the factor of 100 keeps the equilibrium constant within the range of published values. However, if the Seinfeld et al., 1986 value is neglected, because it has been more recently updated in further works of the same author, this argument is

no longer true and the value needed to bring their observations into agreement with E-AIM modeling is an order of magnitude outside of published values.

Taking this into account, the range of effective equilibrium constant values is slightly smaller, only over one order of magnitude, between 1.9x 10^6 – 3.5 x 10^7 mol^2 kg^{-2} atm^{-1} at 298K**.** Although the number of functions that predict a lower value of the effective equilibrium constant (~ 1x 10^6 mol^2 kg^{-2} atm^{-1}) is larger, this is because they are derived, using different methods, from the same thermodynamic measurements reported in Wagman et al., 1982, as is the ISORROPIA II default equilibrium constant for HCl. Therefore, the number of publications quoting one end of this value cannot be used as a good metric of the confidence in a singular effective equilibrium constant value, since they are all based on a single data source.

There are very few measurements of the thermodynamic parameters needed to calculate the effective equilibrium constant of HCl, and all were made before 1965, upon which all of the functions shown here, except Dean et al., 1992, are based. It would be beneficial to further

a)

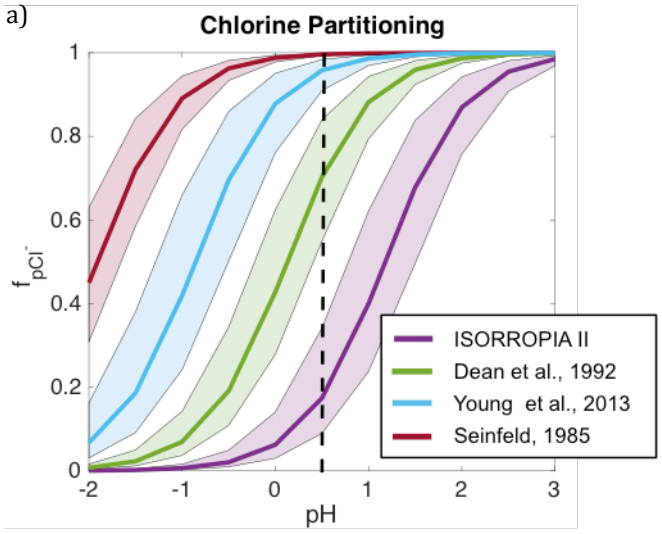

b)

At T=273 K , pH= 0.5, LWC= 1 x 10^{-6} g m^{-3}	f_{pCl^-}
Carslaw et al. (1995), Wagman et al. (1982), Brimblecombe & Clegg (1989)	0.1298
Graedel & Goldberg (1983)	0.5676
Dean (1992)	0.6002
Marsh & McElroy (1985)	0.1267
Young et al. (2013) – NACHTT	0.9355
Seinfeld (1986)	0.9939
ISORROPIA II	0.118

Figure 15: **a)** Figure showing the predicted fraction of chloride in the particulate as a function of pH for four different effective equilibrium constants. Shading shows the values possible for that function between the temperature range 265K-298K, while the solid line shows its value at 273K. The dashed line shows pH=0.5 for which values are quoted in the table shown in Panel B **b)** Table showing the fraction of chloride in the particulate as predicted by all of the functions at T= 273K, pH= 0.5, and LWC= 1 x 10^{-6} g m^{-3}

research involving the impact of halogens in the troposphere, if new data were taken using modern technology to constrain the value of the effective equilibrium constant for HCl.

Figure 15 shows the predicted fraction of chloride as a function of pH at particle liquid water content of 1.0 x 10^{-6} g m^{-3} for several of the different effective equilibrium constants over the temperature range 265-298K. Here it can be seen that the Seinfeld, 1986 value, which has since been revised, and the Young et al., 2013 value would both predict that > 93% of the total chloride present would be in the particle during standard WINTER temperatures, liquid water contents, and pHs. Because such high levels of HCl(g) were observed during WINTER, the chlorine equilibrium defined by such a high effective equilibrium constant would imply extremely high levels of particle chloride must be present, indicating furthermore, that these values are likely too high to be realistic. For example, if the WINTER marine boundary layer median HCl of 1014 pptv only represented 7% or less of the total chloride, as the largest two functions would suggest, then more than 21 μg m^{-3} of chloride would have to be present in the particle phase at STP, which is much greater than observations suggest, even including the coarse mode contributions.

The default ISORROPIA II effective equilibrium constant value is the lowest of all published values at 273 K, and raising it would put more of the total chloride into the particle at equilibrium $\left([Cl^-(aq)] = \frac{K_{eq}\,[HCl(g)]}{[H^+]}\right)$. However, the default ISORROPIA II equilibrium constant in the *Base +Cl* run, already overestimated the amount of chloride in the particle relative to the measurements. Therefore, raising the effective equilibrium constant value at 273K in ISORROPIA II towards literature values would only bring the model into more disagreement with the WINTER measurements by predicting a higher amount of particle chloride present.

Using ISORROPIA II to predict the particle pH, liquid water content and activity coefficients, it is possible to compare the implied equilibrium constant from the WINTER data to that which is currently in ISORROPIA II and other values published in the literature. **Figure 16** shows the comparison of the WINTER data's implied equilibrium constant when the Base + Cl predicted pH, liquid water content, and activity coefficients are used with the CIMS HCl measurement and AMS submicron chloride measurement in the following expression:

$$K_{eq} = \frac{[H^+][Cl^-]}{[HCl]} \left(\frac{\gamma_{Cl}}{LWC}\right)^2$$

where K_{eq} is in units of $mol^2 \cdot kg^{-2}_{soln} \cdot atm^{-1}$, $[H^+]$, $[Cl^-]$, and [HCl] are in $mol \cdot m^{-3}_{air}$ and LWC in units of $kg \cdot m^{-3}_{air}$, and γ_{Cl} is unitless.

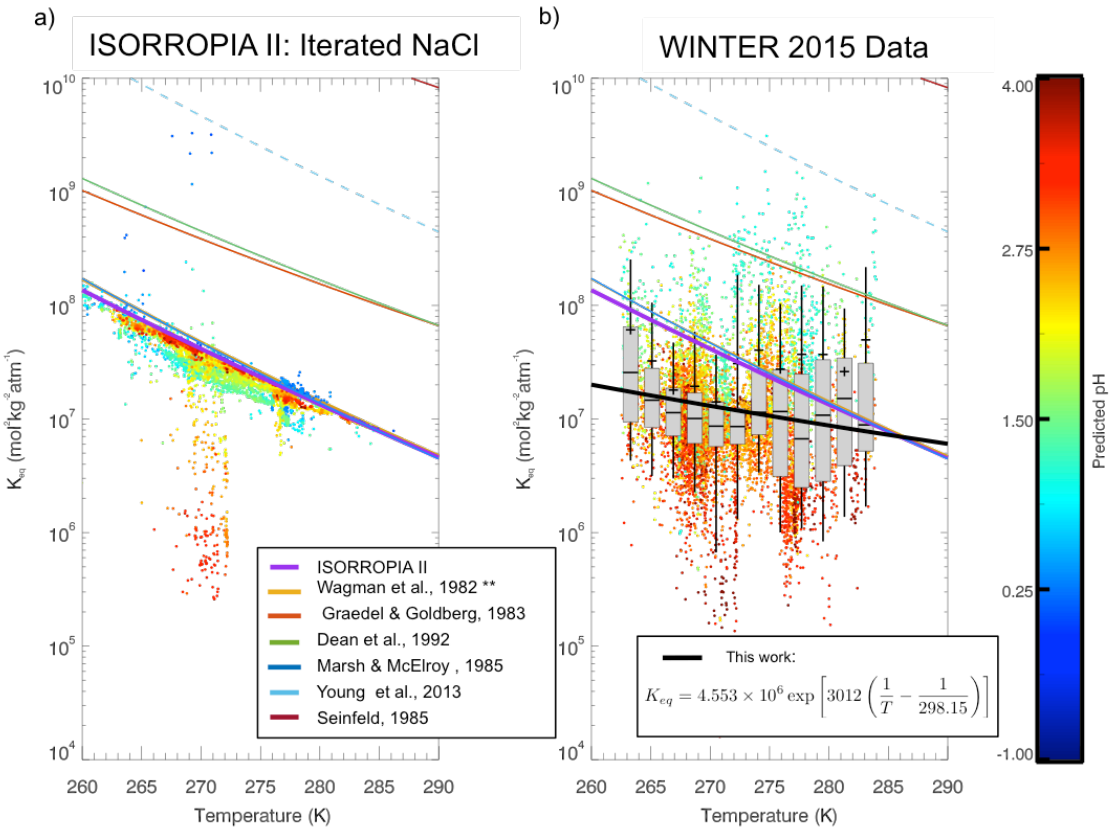

Figure 16: **a)** Figure showing the implied equilibrium constant as a function of temperature, colored by pH from the outputted ISORROPIA II HCl and Cl^- concentrations, pH, LWC, and activity from the *Iterated NaCl* simulation compared to literature functions assuming ideality and activity coefficients equal to 1 **b)** The implied equilibrium constant as a function of temperature, colored by predicted pH, from the measured HCl and Cl^- concentrations during WINTER and ISORROPIA II predicted pH, LWC, and activity coefficients from the *Base+Cl* simulation. Box and whisker plots show the medians of data within a selected temperature range.

**Function also derived in Brimblecombe & Clegg, 1989 and Carslaw et al., 1995

Panel A in **Figure 16** shows that the implied equilibrium constants after the ISORROPIA II Iterated NaCl simulations have been completed. In this simulation, sodium chloride was added until the total chlorine partitioning matched, thereby forcing the equilibrium constant to be correct. The only reason for deviation from the ISORRROPIA II function shown in the key is that the function assumes the solution is ideal and the activity coefficient to be 1, whereas, for many of the lower pH cases, that is not true. It is also possible to apply the same method to the actual WINTER data in order to extract an implied equilibrium constant that was observed during the campaign. By fitting an exponential to the median of the data binned by temperature during the WINTER campaign for conditions in which the equilibrium constant was not affected by extremely large or extremely small values (i.e. HCl > 100 pptv, Cl^- > 0.01 μg•m^{-3}, and LWC > 0.5 μg•m^{-3}, and $\gamma_{Cl} < 3$), a function was derived that represents the median equilibrium constant observed during WINTER. Shown in black in **Figure 16,** the observation-based equilibrium constant was found to be:

$$K_{eq} = 4.553 \times 10^6 \exp\left[3012\left(\frac{1}{T} - \frac{1}{298.15}\right)\right] \qquad \left(mol^2 kg_{soln}^{-2} atm^{-1}\right)$$

Notably, this function does not significantly change the implied value of the equilibrium constant at 298 K, it suggests raising it slightly from the value currently within ISORROPIA II, 1.916 x 10^6 mol^2•kg^{-2}_{soln} •atm^{-1} to 4.553 x 10^6 mol^2•kg^{-2}_{soln} •atm^{-1}, which is well within the range of published values, even excluding the two highest functions. However, the WINTER data suggests a significantly lower temperature dependency of the equilibrium function of 3012 K^{-1} compared to the published literature values of ~6800-9200 K^{-1}.

It should be noted that this function was derived using chloride measurements that do not contain contributions from sea-salt. If the true amount of particle chloride is slightly larger than what was measured by the AMS, then the implied equilibrium constant would actually increase,

thereby bringing it into closer agreement with published literature functions implying that this is, ultimately a lower limit of the effective equilibrium constant for HCl.

The ideal ambient data set collected to use in this work would be size resolved aerosol composition of all anions (Cl^- SO_4^{2-}, NO_3^-) and cations (NH_4^+, Na^+) and gas phase contributions of HCl, HNO_3, and NH_3 at a high time resolution, with low detection limits for all, and that was able to detect both non-refractory and refractory contributions from sea salt components. The AMS data used in all ISORROPIA II simulations, while precise, do not consider the contributions to submicron chloride from sea-salt. And even the estimates of the amount of submicron sodium chloride derived from the *iterated NaCl* simulation are only valid if the equilibrium constant for chlorine partitioning is correct in the model. With a more accurate, and simultaneous measurement of particle and gas phase compounds used in this analysis that did contain sea-salt contributions of particle chloride, the remaining uncertainty in the value of the effective equilibrium constant of HCl could be resolved.

This work illustrates that small pH changes can significantly impact the chorine partitioning, because HCl is more sensitive pH changes than its other counterparts, it is partitioned to the gas phase first as pH changes. The results presented herein highlight the need for the development of a simultaneously precise, accurate, and comprehensive measurement of aerosol ionic composition, with low limits of detection at high time resolution to definitively constrain the phase partitioning of reactive chlorine. While the disagreement in ISORROPIA II's ability to reproduce the observed gas-particle chlorine partitioning during WINTER can be explained by small amounts of missing sodium chloride, it cannot rule out the possibility that the effective equilibrium constant for HCl is incorrect and that the temperature dependency of the function should be lowered. This work specifically demonstrates the sensitivity of this chemistry

to small uncertainties that could, ultimately, change the conclusions of the results presented if such new comprehensive data sets are taken and used to extract meaningful information on the thermodynamics of chlorine partitioning Ultimately, although previous studies have concluded that the inclusion of submicron sea salt components does not impact fine particle pH significantly enough to impact the model's ability to precisely and accurately predict nitrate partitioning [Guo et al 2017], which are reconfirmed here, I have presented evidence that those same impacts *are* enough to sway its ability to accurately predict fine particle chlorine partitioning, which is more sensitive and derived a function for the effective equilibrium constant observed during the WINTER campaign.

6 CONCLUSION

A new comprehensive data set of reactive chlorine observations in the troposphere is presented here. It is in good agreement with most prior literature data, and is available to use for constraints on attempts to model reactive tropospheric chlorine chemistry and its far-reaching impact on air quality and climate. Over both the ocean and land, the overall inorganic chlorine budget was dominated by gas phase HCl and particulate chloride. The total amount of all inorganic chlorine compounds was nearly 3 times larger over the ocean than over land within the bottom 1.5km of the atmosphere. Submicron chloride was a significantly larger percentage of the overall particulate chloride sampled over continental regions than it was over land. Elevated levels of HCl(g) routinely upwards of 500 pptv are seen below 1.5km over the ocean when compared to continental regions with the exceptions of very large directly emitted plumes from power plants that can easily exceed 1 ppbv. Observations show 0-20% of available, submicron non-refractory chlorine partitions into the particle (0 - 0.2 $\mu g\ m^{-3}_{amb}$) at sufficiently high relative

humidities, low temperatures, and pH above 0.8. Although, the thermodynamic model of the system initially significantly over-predicted the amount of chloride in the particle and under-predicted gas phase HCl, suggesting instead, that 20-50% of the total available, non-refractory chlorine should be found in the particle (up to 0.5 μg m^{-3}_{amb}), the discrepancy could be explained by small amounts of fine-mode refractory sources of chlorine, like sea-salt that the measurements could not capture. As **Figure 10** demonstrates, the amount of additional sodium chloride needed to explain the model-measurement disagreement in gas-particle chloride partitioning is less than what the PILS would be able to detect for nearly all of the flights during the WINTER campaign. Therefore, a reasonable amount of fine mode aqueous sodium chloride could explain the chlorine partitioning disagreement without significantly perturbing the nitrate partitioning (or overall aerosol pH). Furthermore, a slight decrease in the temperature dependency of the HCl effective equilibrium constant function used in ISORROPIA II could also explain the model-measurement discrepancy. The function derived for the equilibrium constant here represents a lowest estimate of it from direction observations in the atmosphere providing a novel constraint on the value. Ultimately this work highlights the sensitivity of the chlorine partitioning in ISORROPIA II to even minor input changes and routinely made assumptions that critically affect the model's ability to accurately predict particle chloride concentrations that must be considered when it is used in a global chemical transport model, like GEOS-Chem, to dynamically parameterize heterogeneous halogen chemistry & its numerous downwind affects on air quality and climate.

7 REFERENCES

Abbatt, J. P. D., Thomas, J. L., Abrahamsson, K., Boxe, C., Granfors, A., Jones, A. E., … Yang, X. (2012). Halogen activation via interactions with environmental ice and snow in the polar lower troposphere and other regions. *Atmospheric Chemistry and Physics*, *12*(14), 6237–6271. https://doi.org/10.5194/acp-12-6237-2012

Ansari, A. S., & Pandis, S. N. (2000). The effect of metastable equilibrium states on the partitioning of nitrate between the gas and aerosol phases. *Atmospheric Environment*, *34*(1), 157–168. https://doi.org/10.1016/S1352-2310(99)00242-3

Bahreini, R., Dunlea, E. J., Matthew, B. M., Simons, C., Docherty, K. S., DeCarlo, P. F., … Middlebrook, A. M. (2008). Design and Operation of a Pressure-Controlled Inlet for Airborne Sampling with an Aerodynamic Aerosol Lens. *Aerosol Science and Technology*, *42*(6), 465–471. https://doi.org/10.1080/02786820802178514

Bannan, T. J., Booth, a M., Bacak, A., Muller, J. B. a, Leather, K. E., Breton, M. Le, … Percival, C. J. (2015). Journal of Geophysical Research : Atmospheres of the role of Cl atom oxidation. *Journal of Geophysical Research : Atmospheres*, *120*, 1–20. https://doi.org/10.1002/2014JD022629

Brimblecombe, P. and Clegg, S. L.: The solubility and behaviour of acid gases in the marine aerosol, *J. Atmos. Chem.*, 7, 1–18, 1988.

Brimblecombe, P. and Clegg, S. L.: Erratum, *J. Atmos. Chem.*, 8, 95, 1989.

Canagaratna, M. R., Jayne, J. T., Jimenez, J. L., Allan, J. D., Alfarra, M. R., Zhang, Q., … Worsnop, D. R. (2007). Chemical and microphysical characterization of ambient aerosols with the aerodyne aerosol mass spectrometer. *Mass Spectrometry Reviews*, *26*(2), 185–222. https://doi.org/10.1002/mas.20115

Carslaw, K. S., Clegg, S. L., and Brimblecombe, P.: A thermodynamic model of the system HCl-HNO3-H2S04-H2O, including solubilities of HBr, from <200 to 328K, *J. Phys. Chem.*, 99,11557–11574, 1995.

Chameides, W. L., & Stelson, A. W. (1992). Aqueous-Phase Chemical Processes in Deliquescent Sea-Salt Aerosols - a Mechanism That Couples the Atmospheric Cycles of S and Sea Salt. *Journal of Geophysical Research-Atmospheres*, *97*(D18), 20565–20580. https://doi.org/10.1029/92JD01923

Chen, C.-C., Britt, H. I., Boston, J. F., and Evans, L. B.: Extension and application of the Pitzer equation for vapor-liquid equilibrium of aqueous electrolyte systems with molecular solutes, *AIChE J.*, 25, 820–831, 1979.

Clegg, S. L. and Brimblecombe, P.: The dissociation constant and Henry's law constant of HCl in aqueous solution, *Atmos. Environ.*,20, 2483–2485, 1986.

Cooper, O. R., Parrish, D. D., Stohl, a, Trainer, M., Nédélec, P., Thouret, V., … Avery, M. a. (2010). Increasing springtime ozone mixing ratios in the free troposphere over western North America. *Nature*, *463*(7279), 344–348. https://doi.org/10.1038/nature08708

Dassios, K. G., & Pandis, S. N. (1999). The mass accommodation coefficient of ammonium nitrate aerosol. *Atmospheric Environment*, *33*(18), 2993–3003. https://doi.org/10.1016/S1352-2310(99)00079-5

Dean, J. A.: Lange's Handbook of Chemistry, McGraw-Hill, Inc.,1992.

DeCarlo, P. F., Kimmel, J. R., Trimborn, A., Northway, M. J., Jayne, J. T., Aiken, A. C., … Jimenez, J. L. (2006). Field-Deployable, High-Resolution, Time-of-Flight Aerosol Mass Spectrometer. *Analytical Chemistry*, *78*(24), 8281–8289. https://doi.org/10.1021/ac061249n

Dibb, J. E., Talbot, R. W., & Scheuer, E. M. (2000). Composition and distribution of aerosols over the North Atlantic during the Subsonic Assessment Ozone and Nitrogen Oxide Experiment (SONEX). *Journal of Geophysical Research*, *105*(D3), 3709–3717. https://doi.org/10.1029/1999JD900424

Dibb, J. E., Talbot, R. W., Scheuer, E. M., Blake, D. R., Blake, N. J., Gregory, G. L., … Thornton, D. C. (1999). Aerosol chemical composition and distribution during the Pacific Exploratory Mission (PEM) Tropics. *Journal of Geophysical Research*, *104*(D5), 5785. https://doi.org/10.1029/1998JD100001

Dube, W. P., Brown, S. S., Osthoff, H. D., Nunley, M. R., Ciciora, S. J., Paris, M. W., … Ravishankara, a R. (2006). Aircraft instrument for simultaneous, in situ measurement of NO3 and N2O5 via pulsed cavity ring-down spectroscopy. *Review of Scientific Instruments*, *77*(3). https://doi.org/10.1063/1.2176058

Erickson, D. J. I., Suezaret, C., Keene, W. C., & Gong, S. L. (1999). A general circulation model based calculation of HCI and CINO2 production from sea salt dechlorination : Reactive Chlorine Emissions Inventory annual production of sea distributions of via direct scavenging or chemical production from The generation of se. *J. Geophys. Res.*, *104*(D7), 8347–8372.

Faxon, C., Bean, J., & Hildebrandt Ruiz, L. (2015). Inland Concentrations of ClNO2 in Southeast Texas Suggest Chlorine Chemistry Significantly Contributes to Atmospheric Reactivity. *Atmosphere*, *6* (Atmospheric Composition Observations), 1487–1506. https://doi.org/10.3390/atmos6101487

Foster, K. L., T. E. Caldwell, T. Benter, S. Langer, J. C. Hemminger, and B. J. Finlayson-Pitts (1999), Techniques for quantifying gaseous HOCl using atmospheric pressure ionization mass spectrometry. *Phys. Chem. Chem. Phys.*, 1999,1, 5615-5621.https://doi.org/10.1039/A907362K

Fountoukis, C., & Nenes, A. (2007). ISORROPIA II: a computationally efficient thermodynamic equilibrium model for K –H 2 O aerosols. *Atmos. Chem. Phys. Atmospheric Chemistry and Physics*, *7*, 4639–4659. https://doi.org/10.5194/acp-7-4639-2007

Fountoukis, C., Nenes, A., Sullivan, A., Weber, R., VanReken, T., Fischer, M., … Cohen, R. C. (2007). Thermodynamic characterization of Mexico City aerosol during MILAGRO 2006. *Atmospheric Chemistry and Physics Discussions*, *7*(3), 9203–9233. https://doi.org/10.5194/acpd-7-9203-2007

Fuchs, H., Dubé, W. P., Ciciora, S. J., & Brown, S. S. (2008). Determination of inlet transmission and conversion efficiencies for in situ measurements of the nocturnal nitrogen oxides, NO3, N 2O5 and NO2, via pulsed cavity ring-down spectroscopy. *Analytical Chemistry*, *80*(15), 6010–6017. https://doi.org/10.1021/ac8007253

Graedel, T. E. and Goldberg, K. I.: Kinetic studies of raindrop chemistry: Inorganic and organic processes, *J. Geophys. Res.,* 88C, 10865–10882, 1983

Graedel, T. E., & Keene, W. C. (1995). Tropospheric budget of reactive chlorine. *Global Biogeochemical Cycles*, *9*(1), 47–77. https://doi.org/10.1029/94GB03103

Guo, H., Xu, L., Bougiatioti, A., Cerully, K. M., Capps, S. L., Hite, J. R., … Weber, R. J. (2015). Fine-particle water and pH in the southeastern United States. *Atmospheric Chemistry and Physics*, *15*(9), 5211–5228. https://doi.org/10.5194/acp-15-5211-2015

Guo, H., Liu, J., Froyd, K., Robert, J. M., Veres, P. R., Hayes, P. L., … Weber, R. J. (2017). Fine particle pH and gas-particle phase partitioning of inorganic species in Pasadena, California, during the 2010 CalNex

Guo, H., Sullivan, A. P., Campuzano-Jost, P., Schroder, J. C., Lopez-Hilfiker, F. D., Dibb, J. E., … Weber, R. J. (2016). Fine particle pH and the partitioning of nitric acid during winter in the northeastern campaign. *Atmospheric Chemistry and Physics Discussions*, (January), 1–33. https://doi.org/10.5194/acp-2016-1158

Hayes, P. L., Ortega, A. M., Cubison, M. J., Froyd, K. D., Zhao, Y., Cliff, S. S., … Jimenez, J. L. (2013). Organic aerosol composition and sources in Pasadena, California, during the 2010 CalNex campaign. *Journal of Geophysical Research Atmospheres*, *118*(16), 9233–9257. https://doi.org/10.1002/jgrd.50530

Jayne, J. T., Leard, D. C., Zhang, X., Davidovits, P., Smith, K. A., Kolb, C. E., & Worsnop, D. R. (2000). Development of an Aerosol Mass Spectrometer for Size and Composition Analysis of Submicron Particles. *Aerosol Science and Technology*, *33*(1–2), 49–70. https://doi.org/10.1080/027868200410840

Jaegle, L., Quinn, P. K., Bates, T. S., Alexander, B., & Lin, J. T. (2011). Global distribution of sea salt aerosols : new constraints from in situ and remote sensing observations. *Atmospheric Chemistry and Physics*, *11*, 3137–3157. https://doi.org/10.5194/acp-11-3137-2011

Jimenez, J. L., Canagaratna, M. R., Donahue, N. M., Prevot, A. S. H., Zhang, Q., Kroll, J. H., … Worsnop, D. R. (2006). Supporting Online Material.

Junge, C. (1958). Concentration of chloride, sodium, potassium, calcium, and sulfate in rain water over the United States. *Journal of Meteorology*. Retrieved from http://www.osti.gov/energycitations/product.biblio.jsp?osti_id=5673072

Katzman, T. L., Rutter, A. P., Schauer, J. J., Glynis, C. L., Catherine, J. K., & Klooster, S. Van. (2010). PM2.5 and PM10-2.5 Compositions during wintertime episodes of elevated PM concentrations across the Midwestern USA. *Aerosol and Air Quality Research*. https://doi.org/10.4209/aaqr.2009.10.0063

Keene, C., & Savoie, D. L. (1998). The pH of deliquesced sea-salt aerosol in polluted marine air, Geophys. Res.Lett. *25*(12), 2181–2184, 1998.

Keene, W. C., Aslam, @bullet M, Khalil, K., Erickson Iii, D. J., Mcculloch, A., Graedel, T. E. (1999). Composite global emissions of reactive chlorine from anthropogenic and natural sources: Reactive Chlorine Emissions Inventory. *JOURNAL OF GEOPHYSICAL RESEARCH*, *104*(20), 8429–8440. https://doi.org/10.1029/1998JD100084

Keene, W. C., Stutz, J., Pszenny, A. A. P., Maben, J. R., Fischer, E. V., Smith, A. M., … Varner, R. K. (2007). Inorganic chlorine and bromine in coastal New England air during summer. *Journal of Geophysical Research Atmospheres*, *112*(10), 1–15. https://doi.org/10.1029/2006JD007689

Kim, Y. P., Seinfeld, J. H., Saxena, P., & Seinfeldz, J. H. (1993). Aerosol Science and Technology Atmospheric Gas-Aerosol Equilibrium I. Thermodynamic Model Atmospheric Gas-Aerosol Equilibrium I. Thermodynamic Model. *Aerosol Science and Technology*, *19*(2), 157–181. https://doi.org/10.1080/02786829308959628

Kimmel, J. R., Farmer, D. K., Cubison, M. J., Sueper, D., Tanner, C., Nemitz, E., … Jimenez, J. L. (2011). Real-time aerosol mass spectrometry with millisecond resolution. *International Journal of Mass Spectrometry*, *303*(1), 15–26. https://doi.org/10.1016/j.ijms.2010.12.004

Laskin, A., Moffet, R. C., Gilles, M. K., Fast, J. D., Zaveri, R. A., Wang, B., … Shutthanandan, J. (2012). Tropospheric chemistry of internally mixed sea salt and organic particles: Surprising reactivity of NaCl with weak organic acids. *Journal of Geophysical Research Atmospheres*, *117*(15), 1–12. https://doi.org/10.1029/2012JD017743

Lawler, M. J., Sander, R., Carpenter, L. J., Lee, J. D., Von Glasow, R., Sommariva, R., & Saltzman, E. S. (2011). HOCl and Cl2 observations in marine air. *Atmospheric Chemistry and Physics*, *11*(15), 7617–7628. https://doi.org/10.5194/acp-11-7617-2011

Lee, B. H., Lopez-hilfiker, F. D., Mohr, C., Kurten, T., Worsnop, D. R., & Joel, A. (2014). Supplemental Information for: An Iodide-Adduct High-Resolution Time-of-Flight Chemical- Ionization Mass Spectrometer: Application to Atmospheric Inorganic and Organic Compounds. https://doi.org/10.1021/es500362a

Li, Q., Zhang, L., Wang, T., Tham, Y. J., Ahmadov, R., Xue, L., … Zheng, J. (2016). Impacts of heterogeneous uptake of dinitrogen pentoxide and chlorine activation on ozone and reactive nitrogen partitioning: Improvement and application of WRF-Chem model in southern China. *Atmospheric Chemistry and Physics Discussions*, 1–30. https://doi.org/10.5194/acp-2016-412

Long, M. S., Keene, W. C., Easter, R. C., Sander, R., Liu, X., Kerkweg, A., & Erickson, D. (2014). Sensitivity of tropospheric chemical composition to halogen-radical chemistry using a fully coupled size-resolved multiphase chemistry-global climate system: Halogen distributions, aerosol composition, and sensitivity of climate-relevant gases. *Atmospheric Chemistry and Physics*, *14*(7), 3397–3425. https://doi.org/10.5194/acp-14-3397-2014

Long, M. S., Keene, W. C., Easter, R. C., Sander, R., Liu, X., Kerkweg, a., & Erickson, D. (2013). Sensitivity of tropospheric chemical composition to halogen-radical chemistry using a fully coupled size-resolved multiphase chemistry/global climate system – Part 1: Halogen distributions, aerosol composition, and sensitivity of climate-relevant gases. *Atmospheric Chemistry and Physics Discussions*, *13*(3), 6067–6129. https://doi.org/10.5194/acpd-13-6067-2013

Lopez-Hilfiker, F. D., Iyer, S., Mohr, C., Lee, B. H., D'ambro, E. L., Kurtén, T., & Thornton, J. A. (2016). Constraining the sensitivity of iodide adduct chemical ionization mass spectrometry to multifunctional organic molecules using the collision limit and thermodynamic stability of iodide ion adducts. *Atmospheric Measurement Techniques*, *9*(4), 1505–1512. https://doi.org/10.5194/amt-9-1505-2016

Malm, W. C., & Day, D. E. (2001). Estimates of aerosol species scattering characteristics as a function of relative humidity. *Atmospheric Environment*, *35*(16), 2845–2860. https://doi.org/10.1016/S1352-2310(01)00077-2

Marsh, A. R. W. and McElroy, W. J.: The dissociation constant and Henry's law constant of HCl in aqueous solution, *Atmos. Environ.*, 19, 1075–1080, 1985.

Mielke, L. H., Stutz, J., Tsai, C., Hurlock, S. C., Roberts, J. M., Veres, P. R., … Osthoff, H. D. (2013). Heterogeneous formation of nitryl chloride and its role as a nocturnal NO<inf>x</inf> reservoir species during CalNex-LA 2010. *Journal of Geophysical Research Atmospheres*, *118*(18), 10638–10652. https://doi.org/10.1002/jgrd.50783

Mielke, L. H., Furgeson, A., & Osthoff, H. D. (2011). S.I.: Observation of $ClNO_2$ in a mid-continental urban environment. *Environmental Science & Technology*, *45*, 8889–96. https://doi.org/10.1021/es201955u

Osthoff, H. D., Roberts, J. M., Ravishankara, A. R., Williams, E. J., Lerner, B. M., Sommariva, R., … Brown, S. S. (2008). High levels of nitryl chloride in the polluted subtropical marine boundary layer. *Nature Geosci*, *1*(5), 324–328. Retrieved from http://dx.doi.org/10.1038/ngeo177

Oum, K. W., Lakin, M. J., & Finlayson-Pitts, B. J. (1998). Bromine activation in the troposphere by the dark reaction of. *Geophysical Research Letters*, *25*(21), 3923. https://doi.org/10.1029/1998GL900078

P Pszenny TM, A. A., Keene, W. C., Jacob, D. J., Fan, S., Maben, J. R., Zetwo, M., … Galloway, J. N. (1993). Evidence of inorganic chlorine gases other than hydrogen chloride in marine surface air EVIDENCE OF INORGANIC CHLORINE GASES OTHIER THAN HYDROGEN CHLORIDE IN h/LARINE SURFACE AIR. *Geophys. Res. Lett. GEOPHYSICAL RF_3EARCH LETrER*, *20*(23), 699–702. https://doi.org/10.1029/93GL00047

Phillips, G. J., Tang, M. J., Thieser, J., Brickwedde, B., Schuster, G., Bohn, B., … Crowley, J. N. (2012). Significant concentrations of nitryl chloride observed in rural continental Europe associated with the influence of sea salt chloride and anthropogenic emissions. *Geophysical Research Letters*, *39*(10), 1–5. https://doi.org/10.1029/2012GL051912

Platt, U., Allan, W., & Lowe, D. (2004). Hemispheric average Cl atom concentration from 13C/12C ratios in atmospheric methane. *Atmospheric Chemistry and Physics*, *4*, 2283–2300. https://doi.org/10.5194/acpd-4-2283-2004

Riedel, T. P., Wolfe, G. M., Danas, K. T., Gilman, J. B., Kuster, W. C., Bon, D. M., … Thornton, J. a. (2014). An MCM modeling study of nitryl chloride ($ClNO_2$) impacts on oxidation, ozone production and nitrogen oxide partitioning in polluted continental outflow. *Atmospheric Chemistry and Physics*, *14*(8), 3789–3800. https://doi.org/10.5194/acp-14-3789-2014

Riedel, T. P., Bertram, T. H., Crisp, T. A., Williams, E. J., Lerner, B. M., Vlasenko, A., … Thornton, J. A. (2012). Nitryl chloride and molecular chlorine in the coastal marine boundary layer. *Environmental Science and Technology*. https://doi.org/10.1021/es204632r

Riedel, T. P., Wagner, N. L., Dubé, W. P., Middlebrook, A. M., Young, C. J., Öztürk, F., … Thornton, J. A. (2013). Chlorine activation within urban or power plant plumes: Vertically resolved ClNO<inf>2</inf> and Cl<inf>2</inf> measurements from a tall tower in a polluted continental setting. *Journal of Geophysical Research Atmospheres*, *118*(15), 8702–8715. https://doi.org/10.1002/jgrd.50637

Saiz-Lopez, A., & von Glasow, R. (2012). Reactive halogen chemistry in the troposphere. *Chemical Society Reviews*, *41*(19), 6448. https://doi.org/10.1039/c2cs35208g

Sander, R. (2015). Compilation of Henry's law constants (version 4.0) for water as solvent. *Atmospheric Chemistry and Physics*. https://doi.org/10.5194/acp-15-4399-2015

Sander, R., & Crutzen, P. J. (1996), *101*(134), 9121–9138.

Sarwar, G., Simon, H., Xing, J., & Mathur, R. (2014). Importance of tropospheric ClNO2 chemistry across the Northern Hemisphere, 4050–4058. https://doi.org/10.1002/2014GL059962.Received

Seinfeld, J. H.: Atmospheric Chemistry and Physics of Air Pollution, Wiley-Interscience Publication, NY, 1986.

Sherwen, T., Schmidt, J. A., Evans, M. J., Carpenter, L. J., Gro??mann, K., Eastham, S. D., … Ord????ez, C. (2016). Global impacts of tropospheric halogens (Cl, Br, I) on oxidants and composition in GEOS-Chem. *Atmospheric Chemistry and Physics*. https://doi.org/10.5194/acp-16-12239-2016

Simpson, W. R., Brown, S. S., Saiz-Lopez, A., Thornton, J. A., & Von Glasow, R. (2015). Tropospheric Halogen Chemistry: Sources, Cycling, and Impacts. *Chemical Reviews*, *115*(10), 4035–4062. https://doi.org/10.1021/cr5006638

Spicer, C. W., Chapman, E. G., Finlayson-Pitts, B. J., Plastridge, R. A., Hubbe, J. M., Fast, J. D., & Berkowitz, C. M. (1998). Unexpectedly high concentrations of molecular chlorine in coastal air. *Nature*, *394*(June 1996), 353–356. https://doi.org/10.1038/28584

Tham, Y. J., Yan, C., Xue, L., Zha, Q., Wang, X., & Wang, T. (2014). Presence of high nitryl chloride in Asian coastal environment and its impact on atmospheric photochemistry. *Chinese Science Bulletin*, *59*(4), 356–359. https://doi.org/10.1007/s11434-013-0063-y

Thornton, J. A., Kercher, J. P., Riedel, T. P., Wagner, N. L., Cozic, J., Holloway, J. S., … Brown, S. S. (2010). A large atomic chlorine source inferred from mid-continental reactive nitrogen chemistry. *Nature*, *464*(7286), 271–4. https://doi.org/10.1038/nature08905

Vogt, R., Crutzen, P. J., & Sander, R. (1996). A mechanism for halogen release from sea-salt aerosol in the remote marine boundary layer. *Nature*, *383*(6598), 327–330. Retrieved from http://dx.doi.org/10.1038/383327a0

Wagman, D. D., Evans, W. H., Parker, V. B., Schumm, R. H., Halow, I., Bailey, S. M., Churney, K. L., and Nuttall, R. L.: The NBS tables of chemical thermodynamic properties; Selected values for inorganic and C1 and C2 organic substances in SI units, *J. Phys.Chem*. Ref. Data, 11, suppl. 2, 1982.

Yienger, J. J. (1999). Correction to "An evaluation of chemistry's role in the winter-spring ozone maximum found in the northern midlatitude free troposphere" by J. J. Yienger et al. *Journal of Geophysical Research*, *104*(D7), 8329.

Young, A. H., Keene, W. C., Pszenny, A. A. P., Sander, R., Thornton, J. A., Riedel, T. P., & Maben, J. R. (2013). Phase partitioning of soluble trace gases with size-resolved aerosols in near-surface continental air over northern Colorado, USA, during winter. *Journal of Geophysical Research Atmospheres*, *118*(16), 9414–9427. https://doi.org/10.1002/jgrd.50655